This is to certify that the
thesis entitled

ENABLING TECHNOLOGY FOR THE USE OF R718 IN A
VAPOR-COMPRESSION REFRIGERATION CYCLE

presented by

BRUCE ERNEST LINDBERG, JR.

has been accepted towards fulfillment
of the requirements for the

M.S. degree in Mechanical Engineering

Major Professor's Signature

9/1/09

Date

PLACE IN RETURN BOX to remove this checkout from your record.
TO AVOID FINES return on or before date due.
MAY BE RECALLED with earlier due date if requested.

DATE DUE	DATE DUE	DATE DUE

ENABLING TECHNOLOGY FOR THE USE OF R718 IN A VAPOR-COMPRESSION REFRIGERATION CYCLE

By

Bruce Ernest Lindberg, Jr.

A THESIS

Submitted to
Michigan State University
in partial fulfillment of the requirement
for the degree of

MASTER OF SCIENCE

Mechanical Engineering

2009

ABSTRACT

ENABLING TECHNOLOGY FOR THE USE OF R718 IN A VAPOR-COMPRESSION REFRIGERATION CYCLE

By

Bruce Ernest Lindberg, Jr.

Water as a refrigerant can be an economical and environmentally conscious alternative to conventional refrigerants. It has a long history of being utilized to cool various things throughout human history and even beyond. From ocean currents and floods to the ice in our drinks, water is perhaps the most natural cooling agent on the planet. In addition to the environmental benefits, the use of water in a vapor compression refrigeration cycle will also be shown to perform thermodynamically very efficient. This, in turn, leads to economical benefits in the realm of power consumption as well as availability.

In fact, water as a refrigerant is already being utilized in commercial applications in Europe, Israel, and South Africa. The current state-of-the-art technology used in these countries is discussed. In addition, the challenges that arise from this technology are also discussed as well as the various characteristics that make water as a refrigerant an attractive alternative to conventional refrigerants used in the US.

Finally, the enabling, innovative technology that can be shown to address these challenges is conveyed. The primary component of this technology includes a novel compressor with a unique, woven impeller design including its novel manufacturing technique. Like many technologies, the exploitation of this research is not limited to the immediate motivating concept of water as a refrigerant, but may also be utilized in other applications such as power generation, propulsion, venting, and more.

To my Loving Grandparents

Jim and Gwen Wright

&

Ernest "Bud" and Marylyn Lindberg

ACKNOWLEDGEMENTS

While conducting this research and compiling my thesis, I have been assisted greatly by many people in one way or another. The efforts to complete this thesis would have been impossible without them, and I would like to take this opportunity to thank them.

First, I want to thank my family and friends for their endless support and patience that they have given to me all my life. My relationships with you are the most important part of my life and have allowed me to be the best version of myself that I could be. Thank you for always being there for me through the joyous times and especially the difficult times.

I would also like to thank the past and present members of the turbomachinery lab at Michigan State. You have made the friendly working atmosphere and have shown the technical skills that has made *our* lab what it is known for. For their direct involvement with the goal water as a refrigerant, I would like to first thank Amir Kharazi and his guidance in introducing me to the lab and the research. Next, I would like to thank Ludek Pohorelsky and the graduate students, Nathan Holden, Mark Mouland, Kristen Papuga, Anirban Lahiri, Neelima Reddy, Qubo Li, Jifeng Wang, Mohit Patil, and Blake Gower for their direct involvement. The research has also benefited from the assistance of talented undergraduate researchers who should be named. They are Allen Eyler, Eric Tarkleson, Jakub Mazur, Paul Allen, Darren Fung, Piere Burk, Devesh Chaphalkar, Joel Darin, Jarreau Jackson, and David Kempf.

I would also thank Michigan State University, the College of Engineering, and the department of Mechanical Engineering for giving me the opportunity to pursue my academic career here. In addition, I would like to thank our chief financers, California's EISG program and ASHRAE for funding the research. A special thanks to my committee members Dr. Abraham Engeda and Dr. Alan Haddow for their valuable time and guidance as well.

Finally, I must thank my advising professor, Dr. Norbert Müller for his invaluable guidance and infinite patience while pursuing my education. Dr. Müller has embraced all of his students and their diverse spectrum of backgrounds, methods, and opinions. He has established a working philosophy that encourages creativity, teamwork, and happiness in an environment where such things come second to results and bottom-line thinking. I am fortunate to have had the opportunity to work with Dr. Müller, and I will forever be grateful for what he has taught me about engineering as well as about life.

PREFACE

The purpose of this thesis is to present the broad research conducted at Michigan State University on the enabling technology for water as a refrigerant (R718). Over several years the author of this thesis has worked as a part of a collective effort consisting of numerous members working toward a common goal. It is the objective of the author, to present his own specific work on the thesis topic in the perspective of a broad "roadmap" of the technology.

Unlike many theses, this work is an overall proof of concept and not an in-depth analysis of a specific area of the technology. Therefore, the intimate details of specific components of this technology are not discussed. Although important to the research, there are no rigorous optimizations of blade design, surface features, specific thermodynamic applications, and the like. This thesis *does* however identify and discusses several different principles, that when employed together, can be shown to be feasible in accomplishing the immediate motivation of enabling water as a refrigerant.

Another unique characteristic that arises from a broad approach to a general research topic is the number of different options to the enabling technology that are explored. This research does not identify and pursue a single solution to a problem with a beginning, middle, and end. This thesis *does* however explore several options and solutions, all of which have their own inherent advantages and disadvantages.

This thesis is organized in individual chapters that are designed to guide the reader throughout the enabling technology. Chapter 1 is an introduction that also outlines the motivation for the technology, followed by Chapter 2 that introduces the refrigeration cycle employed. Subsequent chapters explain the challenges, advantages, and specifics

R718, plus representative cycle calculations. Chapter 6 summarizes the current state-of-the-art R718 technology and how it addresses the challenges outlined in Chapter 4. Going beyond the state-of-the-art, a more advanced solution is presented that may enable R718 in widespread use. This advanced solution is a compressor design that is described in Chapters 7 and 8.

Chapter 10 describes the physical realization of the design. To assist with this, a summary of theoretical and numerical work was added in Chapter 9. This chapter is a short compilation of the work of Anirban Lahiri. In Chapter 12, recommendations of further study are given to convey ideas that have not yet been pursued, as well as re-iterate the importance of an older concept that has not yet been realized - the condensing wave rotor first investigated by former research group member, Amir Kharazi.

Table of Contents

LIST OF TABLES

LIST OF FIGURES

Images in this thesis are presented in color.

CHAPTER 1 : INTRODUCTION

The initial motivation of the research presented in this thesis is for the application of water as a refrigerant (R718) for conventional, residential use in the United States. Water may be the most natural cooling agent on the planet. It is a substance that is essential to preserving life-itself, and as will later be demonstrated, can also be used to preserve our quality of life as well.

The need for refrigeration is essential for modern civilization. These needs include, but are not limited to, food and tissue preservation, chemical environments for use in medical and science industries, and air conditioning. Refrigeration can be defined as any heat transfer process that reduces the temperature of an object or location below that of its surroundings [1]. However, the scope of this thesis will be restricted to refrigeration in a vapor compression cycle.

For a perspective on the demand for residential air conditioning, as well as its impact on the environment and economy, a look at the state of California makes logical sense. Perhaps no state in the U.S. is more recognized as being at the forefront of the energy battle than California. The rolling black-outs of 2000 and 2001, economically-crippling energy prices, and increasing demand for air conditioning prompt new innovation in the area of air conditioning and refrigeration. Already in 1997, 96% of the households in California used electric air-conditioning and 30% of peak electricity usage in California is due to air-conditioning [2].

CHAPTER 2 : BACKGROUND

The Vapor-Compression Refrigeration Cycle

Refrigerators, heat pumps, and air conditioning systems operate on cycles called refrigeration cycles. There are many types of refrigeration cycles. Some examples are gas refrigeration, cascade refrigeration, absorption refrigeration, and thermoelectric refrigeration cycles. However, the most frequently used refrigeration cycle is the *vapor-compression refrigeration cycle* [3]. In this refrigeration cycle, the working fluid or heat transferring medium is called the refrigerant. This refrigerant is throttled through four major components of a vapor compression refrigeration cycle and uses the process of latent heat rejection and absorption during phase changes. The four components are:

1. Compressor- where the refrigerant in vapor form is compressed and work-energy is inputted to the cycle
2. Condenser- where heat-energy is rejected to the environment as the refrigerant is condensed
3. Expansion valve- where the cycle is throttled by expanding the refrigerant
4. Evaporator- where latent heat is absorbed by the refrigerant as it is evaporated

This cycle with its components is shown schematically in Figure 1. A common measure of how a cycle like this performs is a dimensionless quantity known as its Coefficient of Performance (COP). COP is defined mathematically as

$$COP = \frac{Q_{in}}{W_{in}} \tag{1}$$

where Q_{out} is the heat absorbed by the evaporator in the cycle and W_{in} is the work input to the cycle. These two quantities may also be expressed on a rate basis. Essentially, the COP is the amount of cooling energy per unit of compressor work energy [1].

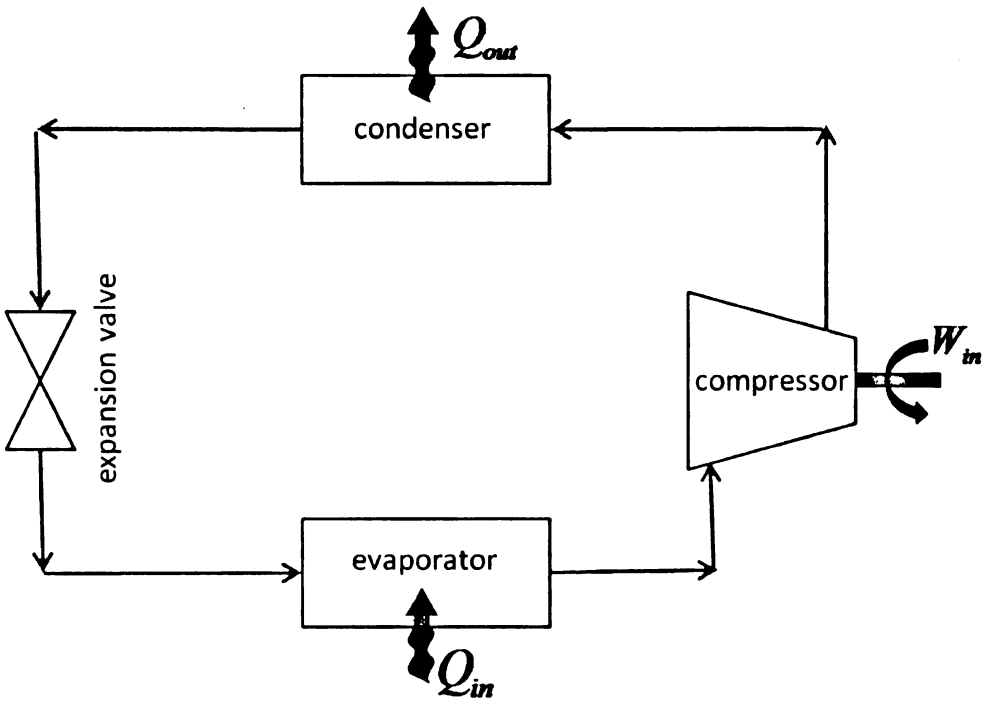

Figure 1. Schematic example of vapor-compression cycle

The Ideal Vapor-Compression Refrigeration Cycle

For simplicity in introducing the vapor-compression refrigeration cycle, an ideal cycle is shown in a T-s diagram in Figure 2. The characteristics of an ideal cycle are:

1. Isentropic compression (1-2)
2. Constant pressure heat rejection and complete condensation (2-3)
3. Isentropic expansion through a throttling expansion valve (3-4)
4. Constant pressure heat absorption and complete evaporation (4-1)

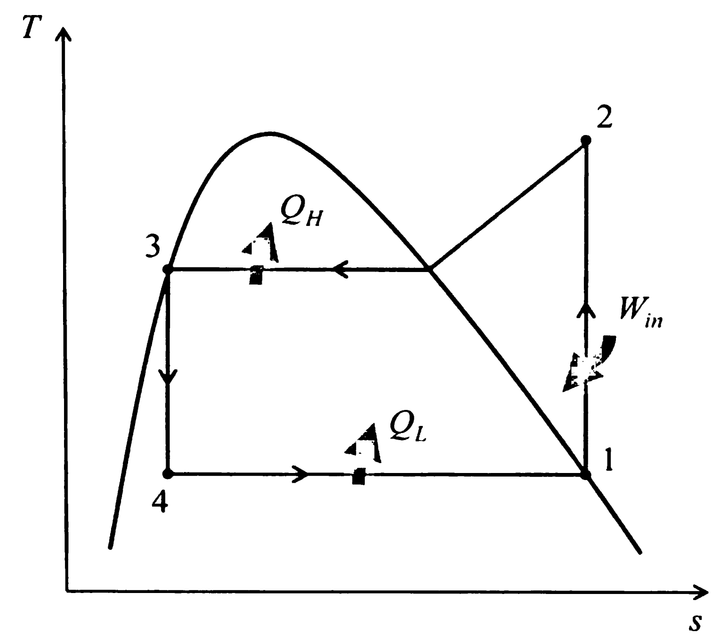

Figure 2. Schematic T-s diagram for the ideal vapor-compression cycle

Although this ideal cycle makes for easy property calculations, it is not practical for describing the cycles that actually occur in the vapor compression refrigeration process. For this, irreversibilities such as heat and pressure losses, as well as super-heating and sub-cooling must be taken into account.

The Actual Vapor-Compression Refrigeration Cycle

The actual cycle differs from the ideal one in many ways. A T-s diagram of this cycle is shown in Figure 3. Numbered points on this figure are also schematically shown in a cycle with system components in Figure 4. Most of the irreversibilities that occur in this cycle can be attributed to pressure losses due to fluid friction as well as heat transfer between system components. The ideal case described above included isentropic compression from 1-2. This involves a compression process that is internally reversible and adiabatic. However in reality, compression results in an increase in entropy shown in process 1-2 in Figure 3. Heat losses during compression can also result in a decrease in entropy as shown in process 1-2' in Figure 3. This non-adiabatic compression is favorable in that it decreases the amount of overall compressor work needed. It is therefore favorable to cool the compression in an actual cycle.

In an ideal cycle the refrigerant is evaporated and condensed to exactly saturated vapor and saturated liquid. In reality however, it is difficult to control the state of the refrigerant so precisely. To ensure complete vaporization before compressing, the refrigerant is slightly superheated in the evaporator before entering the compressor. Likewise, to ensure complete condensation, the refrigerant is also slightly subcooled.

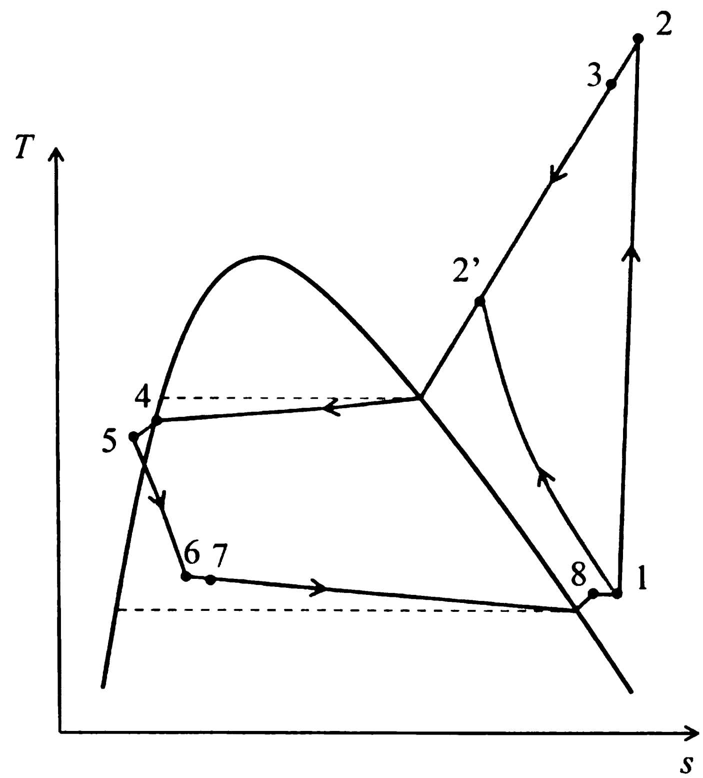

Figure 3. Schematic T-s diagram for the actual vapor-compression cycle

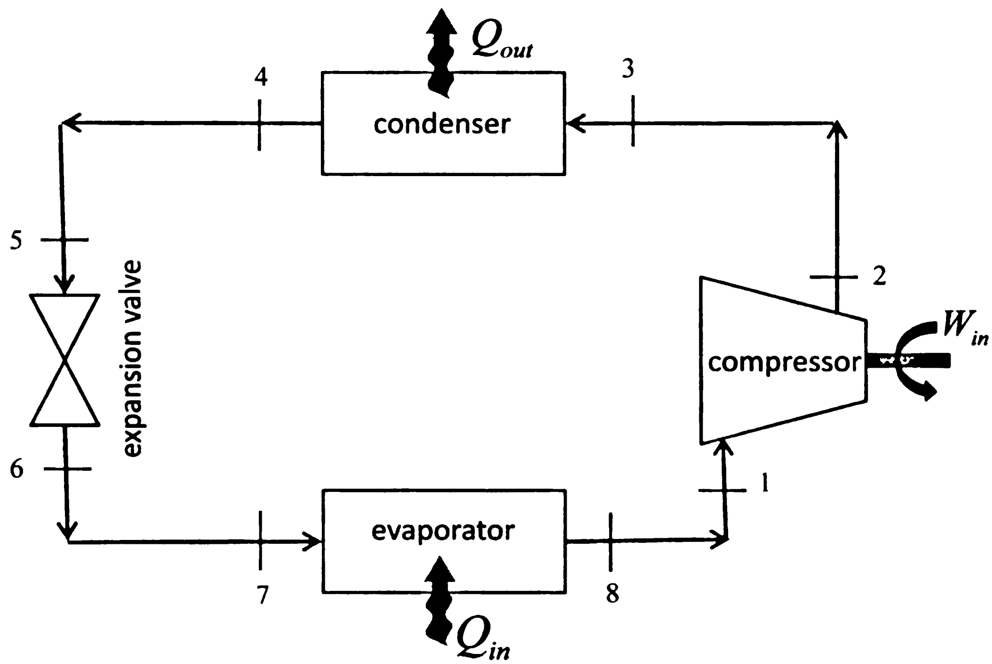

Figure 4. Schematic example of actual vapor-compression cycle with system components

Refrigerants

A refrigerant, in the case of a vapor compression cycle, can be defined as the medium that absorbs and releases thermal energy to and from two dissimilar environments [1]. This refrigerant should possess certain chemical, physical, and thermodynamic properties that render it safe, effective, and economical to use. More specifically the refrigerant should be nontoxic and nonflammable in its pure state or when mixed with air. In addition, the refrigerant should not react unfavorably with system components such as construction materials, lubricating oil, and moisture in the system. Lastly, but not in importance, a refrigerant should be economically attractive as well as environmentally safe, not only in its acquisition, manufacture, and transport, but also its inevitable disposal.

While many substances possess one or more of these characteristics, several do not possess all of them, hindering the substance's applicability. For instance, in the early days of mechanical refrigeration, ammonia (R717) was widely used. Although ammonia is a natural substance, has a low boiling point at atmospheric pressure, and has thermally shown to operate very well in a refrigeration cycle, it is very toxic. This makes this particular refrigerant extremely dangerous and limits its applicability to highly controlled commercial applications. In the late 1920's synthetic refrigerants were developed that were safe, non-toxic, and non-flammable. These compounds are known as chlorofluorocarbons (CFC's). In the 1970's it was shown that CFC's depleted the ozone layer and in 1987 the Montreal Protocol was signed and the manufacture of CFC's was phased out by 1996 [1]. Another synthetic refrigerant, 1,1,1,2-tetrafluorethane (R134a), is one of the leading candidates to replace these CFC refrigerants [1]. R134a is non-flammable, non-explosive, non-toxic, and has no ozone depletion potential (ODP). However, it does have some global warming potential (GWP) because of a small green-house effect.

CHAPTER 3 : BENEFITS OF WATER AS A REFRIGERANT

Often for simplicity's sake, several textbooks introduce the refrigeration cycle to novice thermodynamics students by using water as the working refrigerant. However, as the lesson continues, students are reminded of water's high saturation temperature at ambient pressures, as well as its low volumetric heat capacity. The lesson then abruptly abandons the use of water and subsides to synthetic refrigerants like R12 and R134a.

Environmental Benefits

To offset the continuous threat of global warming and ozone depletion, regulations and bans of traditional refrigerants have been handed down by governments and agencies, namely the Montreal Protocol signed by 57 industrialized countries in 1987. Because of these regulations, the investigations of natural refrigerants such as water are becoming more necessary. Water being completely inert to the environment has many environmental advantages over traditional refrigerants. It has no global warming potential (GWP = 0) and no ozone depletion potential (ODP = 0). In addition, it is non-toxic, and non-flammable. Water can easily be disposed of and needs no manufacturing or extensive refining. While traditional refrigerants meet today's restrictions and standards, it is almost inevitable that these restrictions are bound to change. Water can be guaranteed not to fall under future restrictions. Also included with the economic benefits, is the thermodynamic efficiency of a R718 cycle. These efficiency gains will be discussed in greater detail later, but undoubtedly reduce the needed energy to operate a chiller using water as a refrigerant.

Economic Benefits

In addition to its many environmental benefits, R718 also includes several economical advantages as well. The first and probably most obvious advantage is the availability of R718. Water covers roughly two thirds of the earth's surface. Special treatments are not needed. Municipal tap water can be used, as well as filtered river or stream water. Treated waste water is another possibility. Since the refrigerant is so readily available, there would be no need to warehouse bulky refrigerant containers. The gross cost of the refrigerant would be less since water needs no manufacturing. R718 also reduces safety precautions by working with low pressure differences (less than 1 atm). This may cut down on insurance premiums.

When discussing economic benefits, it is most important to include the energy efficiency of R718 cycles. Thermodynamically, water can be shown to achieve a high coefficient of performance (COP). In studies, the COP is shown to be 20-30% higher than conventional refrigerants [4]. Unlike other refrigerants, R718 can be used in direct heat exchangers, increasing the efficiency of the cycle even more. This technology will be discussed later in Chapter 5.

CHAPTER 4 : CHALLENGES OF WATER AS A REFRIGERANT

Just as R718 can be shown to be beneficial as a refrigerant, there are also several key characteristics that complicate its immediate application in refrigeration cycle, and are outlined as follows:

Working Under Vacuum

As explained in Chapter 2 of this thesis, the vapor compression cycle works by absorbing heat from a cold space during a phase change. That is to say, as heat is absorbed from the cold space to the *evaporator*, the refrigerant then *evaporates* or boils. A novice student of elementary science can tell you that at standard pressure, water evaporates at 100°C. However, as pressure decreases, water evaporates at lower temperatures. Since most applications require heat removal at temperatures well below ambient temperatures, cycles using R718 must be ran at low pressures under a coarse vacuum.

Working under vacuum comes with its own inherent challenges. A pump must evacuate piping in the cycle and sealing must be employed to maintain the low pressure. Challenges in sealing may occur at joints and couplings within the cycle. Many systems are pressurized and the challenge is to contain the contents from escaping into the ambient environment. However under vacuum, it is a task to keep the ambient environment from contaminating the system. In addition, most mechanical and electrical components are designed for operation under ambient pressure. Their immediate application may need to be modified for use under ultra-low pressure.

Large Volume Flows

Since the cycle works under vacuum pressure, the volumetric cooling capacity of water vapor is very low. Hence a cycle using R718 needs a larger volume flow of about 200 times higher than traditional refrigerants. That being said, the majority of turbo compressors for refrigeration are centrifugal or mixed-flow, and although capable of achieving greater pressure ratios per stage, these types of compressors are not suited for high volume flows.

High Pressure Ratios

Due to the thermodynamic properties of water vapor, its application in a refrigeration cycle requires a high pressure ratio to be achieved. This pressure ratio is about double, or triple that of a cycle using traditional refrigerants like R134a or R12. A comparison of properties like this can be shown in Table 1 below. It should be noted that calculations in this table were done using an evaporator temperature of 10°C and a condenser temperature of 50°C.

Low Reynolds numbers

Due to the high pressure ratio required, turbo impellers need to have approximately two to four times higher circumferential speed, depending on the impeller design. The speed of sound is approximately 2.5 times higher, so material limitations are of more concern than Mach number restrictions. Reynolds numbers are like 300 times lower and the specific work transmission per unit mass has to be around 15 times higher. [5], [6], [7].

Table 1. Refrigeration comparison chart [7]

Refrigerant	ODP	GWP	Capacity [kJ/kg]	Pressure Ratio	Compressor Temp out [°C]
R718	0	0	2309.0	10.0	223
R717	0	0	102.9	3.03	99
R12	1	8500	106.5	2.88	55
R22	0.034	1900	145.6	2.85	67
R290	0	20	250.1	2.66	54
R134a	0	1600	131.9	3.18	62
R152a	0	190	228.0	3.15	52

CHAPTER 5 : THE CYCLE

To describe the characteristics of water used in a vapor compression cycle, as well as to demonstrate the performance of R718, a cycle analysis was conducted. When describing any vapor compression cycle calculation, it is important to first disclose the assumptions made. To make the calculations as straightforward as possible, several simplifying assumptions were made, and are as follows:

1. Compression is done in a single stage.
2. There is no superheating or sub-cooling.
3. There are no pressure losses in the piping and no energy transfer to the environment.

The cycle was calculated with Microsoft Excel using an assumed polytropic efficiency. Properties such as temperature, pressure, enthalpy, and entropy, were calculated at each of four different stages in the refrigeration cycle. These stages were the evaporator, compressor, condenser, and expansion valve. Using the pressure ratio obtained, from these calculations, an isentropic efficiency was calculated based on the formula

$$\eta_{isentropic} = \frac{\Pi^{\alpha} - 1}{\Pi^{\left(\frac{\alpha}{\eta_{polytropic}}\right)} - 1} \tag{2}$$

Here $\eta_{polytropic}$ is the assumed polytropic efficiency, Π is the pressure ratio, and α is the isentropic exponent or

$$\alpha = \frac{\kappa - 1}{\kappa} \tag{3}$$

where κ is the ratio of specific heats.

$$\kappa = \frac{c_P}{c_v} \tag{4}$$

With the new calculated isentropic efficiency, properties were iteratively re-calculated to reflect better accuracy. Using these properties, the cooling load and compressor work were calculated and thus the COP could be calculated by equation (1).

Mapping COP and pressure ratios

As with calculating the COP of any refrigeration cycle, the COP varies with properties and cycle characteristics. Two important properties that affect COP are the evaporator temperature as well as the condenser temperature. This is intuitive since one would expect a cycle to be more efficient the less cold the "cold space" needed to be. By the same logic, one would also expect better efficiency the colder the ambient space the heat was rejected to was. Since the evaporator and condenser temperatures are perhaps the first criteria when designing a refrigeration cycle, COP values were plotted with respect to these criteria.

Plotting COP versus evaporator temperature alone fails to convey the effects of condenser temperature on COP. Likewise, plotting COP versus condenser temperature alone doesn't describe the effects of the evaporator temperature on COP. To essentially describe three parameters simultaneously, COP iso-lines were plotted for evaporator temperature versus temperature lift from condenser to evaporator. This was done by using a Visual Basic code to locate combinations of evaporator temperature and temperature lift that yield a particular COP value. Integer COP values from 2 to 10 were used and iso-lines were mapped. A base line plot of this using R718 as the refrigerant is shown in Figure 5. Here one can see the large operating range of R718 as well as the general trend for decreasing COPs with increasing temperature lift. The vertical yellow line represents the optimum operating temperatures to maximize COP. These optimal temperatures indicate high efficiencies for R718 in the case of using a heat pump.

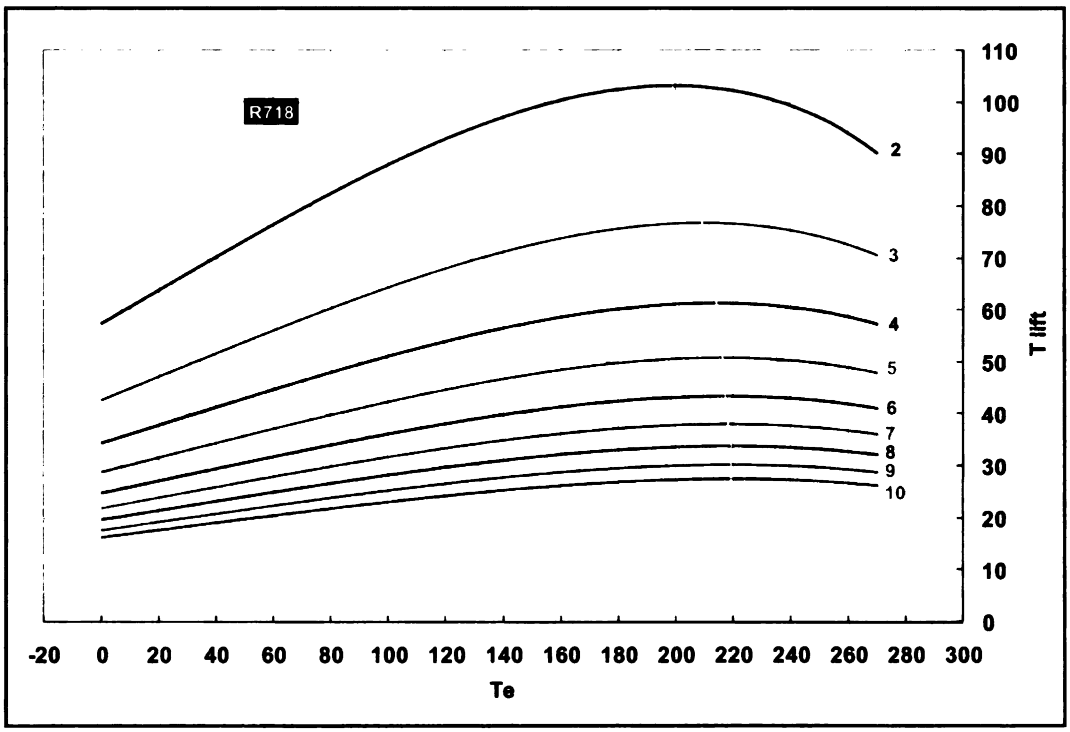

Figure 5. COP iso-lines for R718 with ηp=0.7

To compare COP values of R718 to other conventional refrigerants, COP iso-lines can be mapped on the same plot such as in Figure 6. In this case, R134a is being compared. It is worth noting the operating temperatures most favorable to R134a as well. The intersection of each refrigerant's iso-lines is marked with a green dashed line. From this, it is shown that for operating temperatures on this line, R134a and R718 have the same COP. Furthermore, one can make the valid assumption that R718 has a higher COP value for operating temperatures to the right of this intersection line. To accentuate this range of operating temperatures favorable to R718, Figure 7 shows a plot zoomed in on this range.

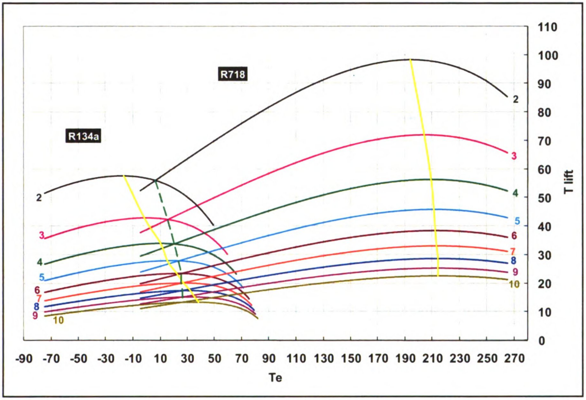

Figure 6. COP iso-line comparison between R718 and R134a with ηp=0.7

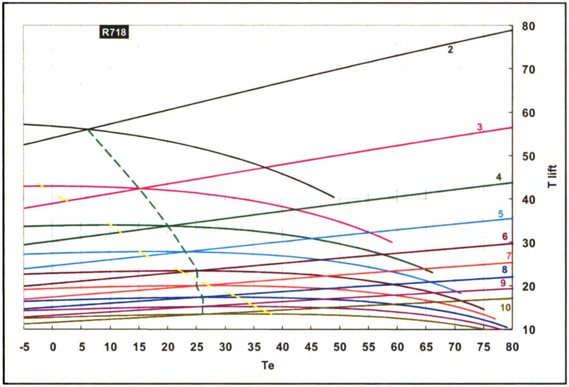

Figure 7. Zoomed-in view of COP iso-line comparison between R718 and R134a with ηp=0.7

Other Factors that impact COP

Heat Exchangers

By Figure 7, it can be argued that the operating temperatures where R718 has a higher COP than R134a is quite limited. However, an important characteristic of the two cycles was neglected. One of the biggest advantages of using R718 is that it may be used in direct heat exchangers. This means that there doesn't need to be such a substantial temperature difference to drive the heat transfer in the evaporator and condenser. The resulting effects are a larger temperature lift needed for the same cooling load. This, in turn, decreases the COP. In the case of R134a, this decrease in COP is much more than for the case using R718. A conservative assumption of the temperature difference needed in R134a heat exchangers would be 5°C. Conversely, R718 would only need a 1°C temperature difference. A demonstration of the effect the different heat exchangers have on their respective COPs can be shown in Figure 8 Here a COP of 5 is used, and one can see the intersection point go from an evaporator temperature of about 35°C to a much lower temperature below R718's operating range. Figure 8 also shows the COP 5 line of R134a dropping well below the R718 line indicating a better COP for R718 at these conditions. A new, more accurate plot of all the COP iso-lines can now be observed in Figure 9. This shows a much larger range of operating temperatures where R718 has a higher COP when compared to the graph in Figure 6. Like Figure 7, Figure 10 shows a zoomed view of these optimal temperatures, but with the heat exchanger effects taken into account. From this, one can assess the fact that with these conditions, R718 has a higher COP than R134a for evaporator temperatures greater than -1°C and for any temperature lift. Another interesting observation is that from this plot it can be deduced that for the particular case of a 12°C evaporator temperature and a 20°C temperature lift, the COP of R718 is 10 and the COP of R134a is 7. This point is demonstrated by the shaded oval in Figure 11.

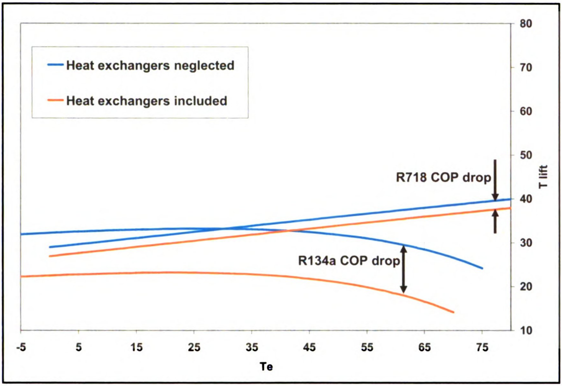

Figure 8. Effect of heat exchangers on COPs of R718 and R134a

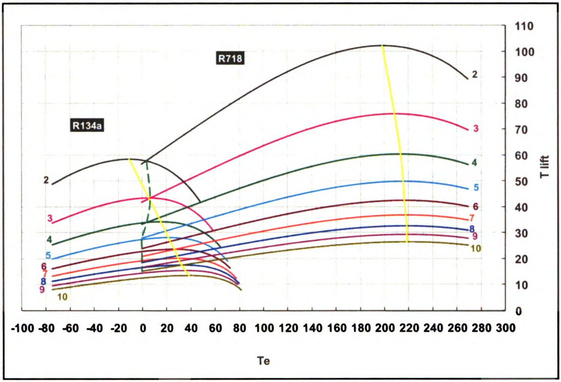

Figure 9. COP iso-line comparison between R718 and R134a with ηp=0.7 including heat exchanger effects

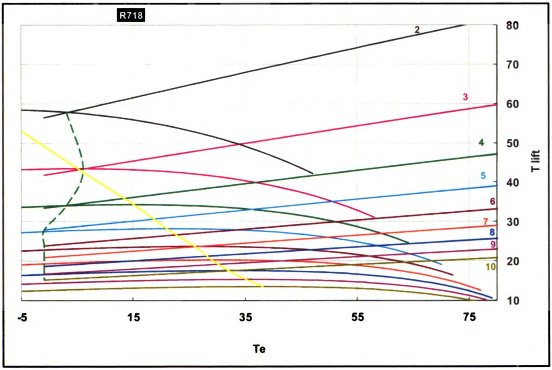

Figure 10. Zoomed-in view of COP iso-line comparison between R718 and R134a with ηp=0.7 including heat exchanger effects

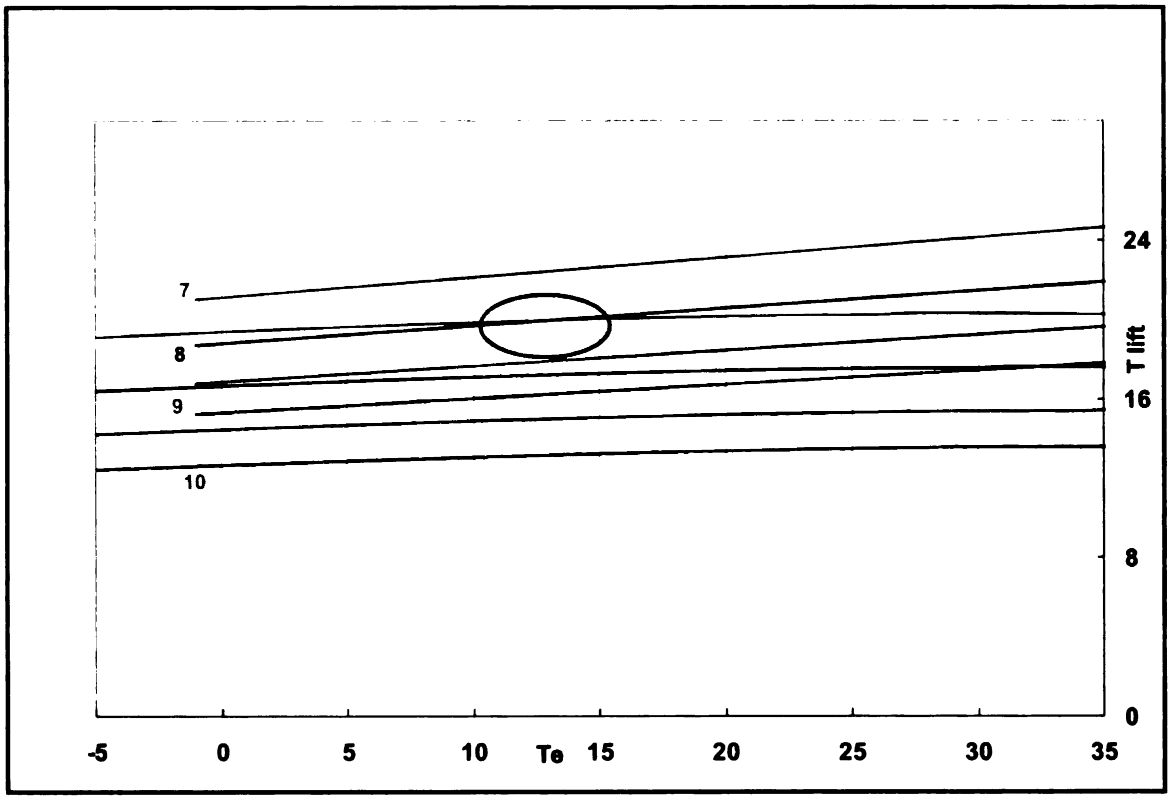

Figure 11. Zoomed-in view of data point in a COP iso-line comparison between R718 and R134a with ηp=0.7 including heat exchanger effects

Polytropic Efficiency

As stated before, the cycle was calculated using an assumed polytropic efficiency. This assumption in itself can have a significant effect on the COP iso-lines. To demonstrate this, COP iso-lines were mapped on temperature ranges as before, except now with an assumed polytropic efficiency of 0.9. This plot can be shown in Figure 12. Again, this plot takes into account the heat exchangers as before. It is evident by Figure 12 that the COP iso-lines for R718 and R134a have both increased. However, as shown in Figure 13, R718 iso-lines have comparatively increased more.

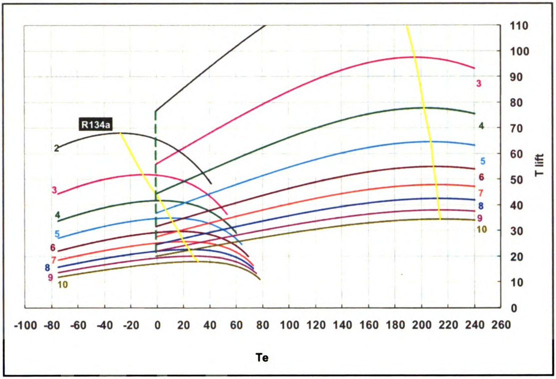

Figure 12. COP iso-line comparison between R718 and R134a with ηp=0.9 including heat exchanger effects

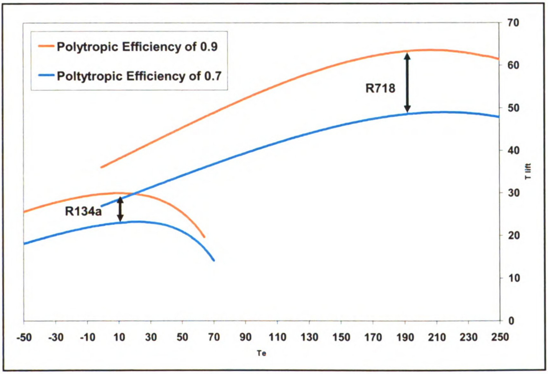

Figure 13. Effect of polytropic efficiency on COPs of R718 and R134a including heat exchanger effects

CHAPTER 6 : CURRENT STATE-OF-THE-ART

Although the above calculations in the previous chapter convey R718 as a viable alternative to traditional refrigerants, the challenges outlined in Chapter 2 must still be addressed. To address the challenges of using water in a compression refrigeration cycle, innovative technology is necessary. The simple application of conventional refrigeration technology and compressors has repeatedly been found to be neither economic nor competitive in the US market [5], [6]. However, R718 units have been installed outside of the U.S. in countries like Germany, Israel, and South Africa as shown in Figure 14. Still, typically the compressors and complete units are deemed to be too expensive, too big, and unable to scale down to smaller capacities below 100 ton.

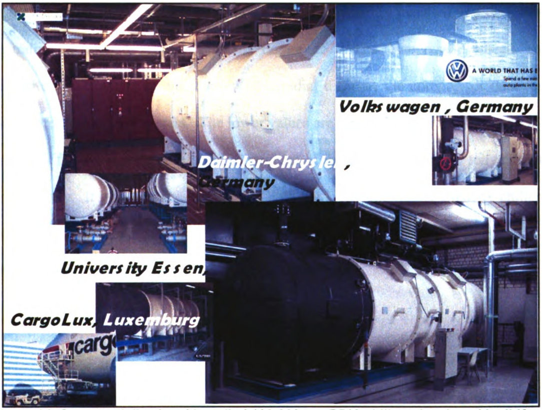

Figure 14. Commercialized and installed 100-300 ton R718 chillers developed by ILK Dresden, Germany

The most important component of a R718 chiller is the compressor. There are world-wide only two companies that have developed and commercialized R718 compressors. The first one is IDE Technologies Ltd., Israel [8] and the second one is at Institut für Luft- und Kältetechnik (ILK) Dresden gGmbH (Institute of Air and Refrigeration), Germany where the Associate Professor Dr. Norbert Müller has been a key engineer in the development effort [9], [10], [11]. Derived from desalination, the larger IDE compressors have also been used for designs by Danish Technological Institute (DTI) and the Sabroe Refrigeration Company in Denmark [12] and by INTEGRAL, Germany [13]. The IDE centrifugal compressors have been developed into two products called ECOVIM (Vacuum Ice Machine) [14] and ECO-CHILLER [15]. Both the IDE and the ILK compressors are of centrifugal diagonal-flow (axial inlet and radial outlet) type with stationary inlet guide vanes, and typically installed in a two stage configuration as shown schematically in Figure 15. The compressor wheels are approximately 1-2 meters in diameter. With a radial diffuser, the compressor diameter reaches approximately 2-4 meters. The lower values are for the ILK compressors and the larger values for the IDE compressors. Capacities of these chillers are 100 ton and 300 ton respectively. It is interesting to note that both the lower and higher capacity chillers have almost the same in technology and price, indicating that these chillers' size and cost do not scale with capacity [16].

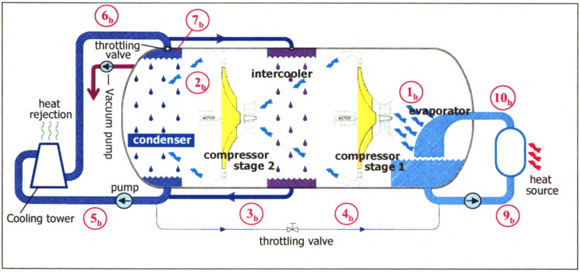

Figure 15. Schematic illustration of the current state-of-the-art R718 refrigeration cycle

The compressor wheels are lightweight constructions with extremely thin blades made of titanium or composite material sheets as illustrated in Figure 16. While energy savings of 20% have been shown with this technology [17], the fluid mechanics design is still much compromised for stability. This indicates the potential for an even more efficient design. The current state of the art impellers are very unique in that they are not milled like usual high-performance impellers. Some of the notable features of these impellers can be shown in Figure 16 and are outlined as follows:

- The blades of these wheels are flat and straight, not aerodynamically curved.
- Same is true for the hub contour that even shows cut backs between the blades.
- Technology does not allow for an outer shroud introducing a tip clearance with leakage flow.
- These state-of-the-art compressors work with stationary guide vanes (IGV) and guide elements in the diffuser that both limit the operating range and introduce friction surfaces that do not transmit compression work.

The features listed above have limited the achieved compression efficiency to about 60 to 70 percent. The wheel assemblies are built from multiple parts in a laborious process [18], [19], [20]. The design is a major reason for the high cost that does not scale with size, making only larger units greater than 100 ton marketable, and this often only in protected markets.

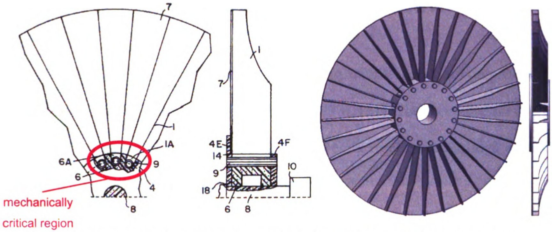

Figure 16. Illustration of current state of the art compressor wheels

Both the IDE and ILK compressors work with a direct electric motor drive. However, two different approaches have been followed. IDE has placed the motor outside of the unit under atmospheric conditions as shown in Figure 17. This addresses the challenge of sealing the shaft. ILK has placed the electric motor drive inside the unit under water vapor atmosphere and vacuum, having resolved the greater challenges of electric insulation, heat removal, and bearings.

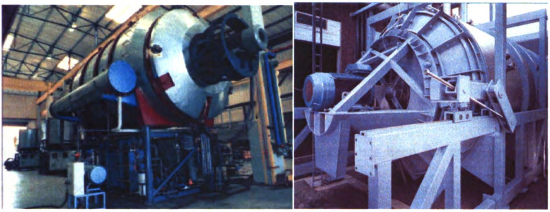

Figure 17. Current state of the art units at IDE, Israel

There has also been the concept of using multistage axial compressors in the HydroFrio™ chiller introduced by INTEGRAL [13], [21]. These compressors have been derived from gas turbine compressors and apparently resulted in too high costs for the HVAC&R market and have not been commercialized.

CHAPTER 7 : ALTERNATIVE COMPRESSOR CONFIGURATION

Axial Flow Compression

Turbo compressors are classified as either axial-flow or radial (centrifugal flow) compressors. Traditionally, the centrifugal compressor has been the more rugged and lower cost-type, while the axial-flow compressor has offered better efficiency. These differences, however, have become much less significant in recent years due to advances in technology, particularly with regard to efficiency [22]. Flow streamlines through axial impellers have a radius that is constant or nearly constant, while in centrifugal impellers, the streamlines undergo a substantial increase in radius. For this reason, centrifugal compressors are able to achieve a higher pressure ratio in a single stage. This can be described mathematically with Euler's equation for turbomachinery shown in equation (5).

$$\tilde{e} = u_2 c_{u2} - u_1 c_{u2} \tag{5}$$

Here $\tilde{e}$ is the specific (per unit mass) shaft work done on the fluid, u_2 and u_1 are the tangential velocity of the impeller at outlet and inlet respectively, and c_{u2} and c_{u1} are the tangential component of the fluid velocity at outlet and inlet. From this equation, it is obvious that a change in radius leads to a change in tangential velocities and in turn, will lead to a larger work transmission.

Although centrifugal compressors are traditionally capable of achieving higher pressure ratios in a single stage, axial compressors can achieve significantly greater mass flow rate per unit frontal area [22]. Also since the radius doesn't increase substantially, axial impellers are much smaller in diameter than centrifugal compressors. An example of this size difference is shown in Figure 18. Here it is shown that the diameter of an axial compressor is one fourth the diameter of a centrifugal compressor with stationary guide vanes. Since area increases with the square of diameter, centrifugal compressors can take up to 16 times the area than axial compressors. Current state of the art industrial water vapor chillers in use in Europe employ centrifugal compressors with typical diameters of around 1 m. By comparison a chiller using an axial flow compressor yielding a similar cooling capacity would have a diameter of around 0.5 m. In a general sense, unit costs reduce with size and become more applicable in cases with tight space constraints.

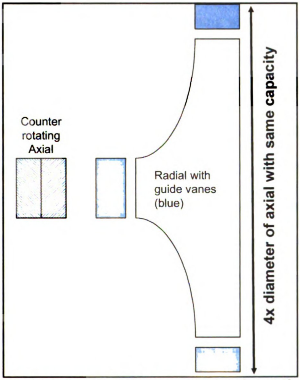

Figure 18. Diameter comparison between axial and centrifugal impellers

Multi-Stage Compression

To achieve the necessary pressure ratios, efficiencies, and Mach number constraints, water vapor must be compressed in multiple stages [23]. In simulations, when the desired pressure ratios are put in place with a single stage compressor, the results are unreasonable. For example, the tip speeds are much too large for most modern equipment. Velocities over 500 m/s are not achievable by most of the widely available materials. The forces placed on the compressor itself, at this velocity, would cause high stresses, this causes the components within the compressor to fatigue quickly or yield. Several configurations are possible to achieve the needed work transmission. These may or may not include stationary guide vanes. An illustration of some possible configurations can be shown in Figure 19. When using water vapor, the compressor exit temperatures tend to be higher than more commonly used refrigerants, and with multiple stages, this temperature change becomes amplified.

Multi-stage compression also allows for inter-cooling. Inter-cooling between stages reduces the required work input to the compressor [3], [23]. This, in turn, increases the overall efficiency of the compressor. It also allows for the temperature of the water vapor to be decreased in between stages; decreasing the overall compression temperature changes. Flash inter-cooling is one of the ways to effectively achieve compression temperature adjustment. With this type of cooling, liquid water is injected into the fluid exiting the compressor. The water is to then to be evaporated by the superheated vapor, bringing the fluid to the saturation temperature. The negative effects are that the mass flow increases between each of the stages [6].

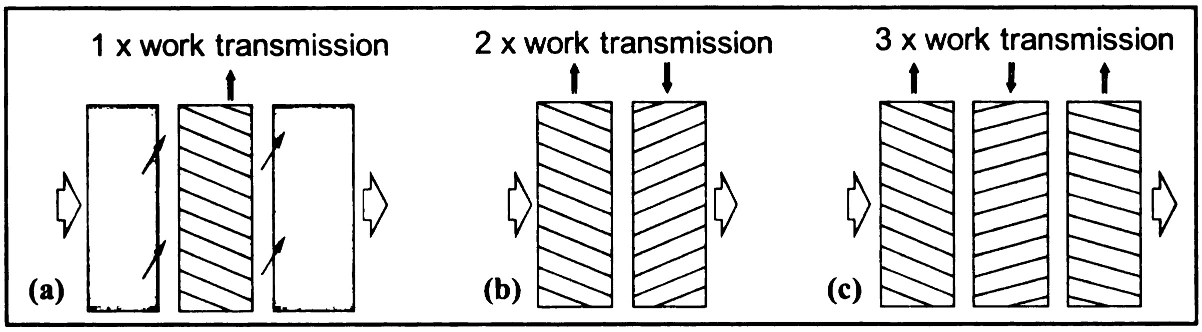

Figure 19. Compressor stage comparison

As explained in Euler's Equation (5), the work transfer comes from the change in the tangential component of the fluid velocity. Because of this, axial compressors often employ the use of stationary guide vanes to add or remove a pre-swirl from the rotating impellers. An example of this configuration can be shown in Figure 19(a). Here the guide vanes in blue introduce a pre-swirl before the impeller, and then remove the swirl after the impeller. There are several reasons for this, an important one is symmetry. If the dynamics of the fluid remain the same throughout each stage of compression, the hardware for each of the compressor stages can be designed the same. The impellers being of the same material, rotating in the same direction, and at the same speed also allows all them to be fixed to the same shaft. This in turn increases the manufacturability of the entire compressor.

Regrettably, with the ease of manufacturability also come difficulties in size constraints. The additional guide vanes between stages require the overall compressor to be much larger to accommodate the additional hardware. However by counter rotating the impellers, these guide vanes can be eliminated. Eliminating these guide vanes makes the compressor smaller and more adaptable to various applications. A direct correlation can also be made between a decrease in price and size reduction. In addition to reduced prices, the hydraulic losses caused by the guide vanes are also eliminated. Removing the need for guide vanes is done by counter-rotating the impellers. This process utilizes the swirl after an impeller stage to gain additional work transmission in the next stage. In equation (5) the work transmission comes from the difference of the tangential velocities of the fluid at inlet and outlet. If the velocities at inlet and outlet are in opposite directions, twice as much work can be transferred to the fluid in a single stage, and thus more compression of the vapor. This is done by rotating the impeller in the opposite direction of the preceding impeller. A schematic example of counter rotation can be shown in (b) and (c). Here one can observe the additional compression for the same size compared with the configuration in (a). This is also known as an increase in power density (work transferred per unit volume).

CHAPTER 8 : NOVEL DESIGN FOR MANUFACTURING

Because of the low density of gases, the majority of the forces seen by the impeller are not from the gas passing through the blades, but forces in its radial direction due to its own inherent mass rotating at high speeds. Because of this, the impeller must be of lightweight and strong material. The impeller being lightweight reduces safety issues that arise from using heavy materials as well as reduces the forces inflicted on the bearings. Lightweight materials also reduce the need for extensive balancing. As stated in Chapter 6, conventional water vapor compressors, have impellers made from titanium or formed composite sheets. Although strong and lightweight, they are made component by component by hand and are time consuming and extremely expensive to manufacture or prototype. To address this issue, new technology being investigated at Michigan State University involves the use of a wound or woven composite impeller.

Composite Materials

In short, a composite material is essentially any material that is made up of high strength fibers arranged in a matrix. The benefits of composite materials are widely known and vast. Most notably are their high strength and low weight which, as noted above, make composite materials particularly attractive for impellers for vapor compression. Composite materials are also anisotropic which allows for the fibers to be arranged in the direction of the highest force. Interestingly, composite materials can be both man-made substances as well and natural materials. Examples of naturally occurring composite materials are wood or bone, whereas examples of man-made composites can be concrete or fiberglass moldings for boats.

Filament Winding

Filament winding techniques has been well investigated over the last thirty years [24], [25]. In a simple description of the process, reinforcement fiber tows in bundle form are fed trough a wet bath wherein they are impregnated with resin, and are then uniformly and regularly wound onto a rotating mandrel. Once the desired architecture and lay up thickness are achieved, the wheel can be cured and the mandrel removed. This technology is typically used for the fabrication of parts that are axial-symmetric, such as pipes, containers, pressure vessels, rocket motor cases, and other tubular structures [24], [25]. Depending on the desired properties of the product, winding patterns such as hoop, helical, and polar can be developed. Various curing system such as drying in the oven, through hot oil, heat by lamps, steam, autoclave and microwave are possible for different applications.

The principal advantages of filament winding are its low labor cost and its reproducibility. This is due to robotic motion via computer coded design. Thus, one can apply this filament winding technology to manufacture composite impellers at a low labor cost. In addition, various weaving patterns can also be achieved. These patterns will be discussed in the following section. Another advantage of filament winding is the ability to interweave motor components. This could be induction wires or magnetic materials dispersed within the matrix. Motor schemes like this will also be discussed in greater detail later.

Fiber Material

In recent years, the fiber material that has perhaps been given the most attention is carbon fiber. This is undoubtedly because of its low density (about 2.268 g/cm^3) and high strength (up to 1000 GPa for single crystal graphite [25]. Certainly properties like these warrant its widespread use in applications such as aerospace, sporting equipment, and auto racing. However, several other fibers exist as well, each with their own intrinsic properties associated with them. Some examples include glass, boron, and organic fibers. The broad vision of this research undoubtedly includes the use of carbon fiber for the characteristics mentioned above. Initial experience has lead to the experimentation with the aramid fiber, Kevlar®.

Kevlar®, based on the chemical poly(p-phenylene terephthalamide) was created in 1965 by DuPont™ originally for the replacement in steel in radial tires, but has been made most famous by its use in bullet-proof fabrics. Although its modulus is less than that of carbon fiber, Kevlar® has a lower density and has proven to be less brittle, which make it useful in a variety of applications. In the case of winding turbo impellers, these properties are favorable since impellers need to be light-weight, and also since patterns sometimes have sharp turns where fibers could break or fray. In addition to these properties, Kevlar® also has a small negative thermal coefficient of expansion that may counter dynamic deflections with thermal contractions at high compressor temperatures. Kevlar® also has good vibration damping characteristics. Composites of Kevlar®/epoxy show about 5 times the vibration dissipation than glass/epoxy composites [25]. There are several types of Kevlar® yarn that have a variety of properties and can be noted in Table 2.

For convenience and availability, dry, spun Kevlar® yarn or thread was obtained for initial prototyping. However, tows made of clusters of entire fibers are also available. The Kevlar® thread was purchased from Atlantic Thread and Supply Company™ out of

Baltimore, MD. Specifically, the thread that purchased and used for this research is CRAQ-SPUN® Tex-35 Glazed which comes in black or natural colors. However, other sizes are available.

Table 2. Properties of Kevlar aramid fiber yarns [25]

Property	K 29	K 49	K 68	K 119	K 129	K 149
Density (g cm^{-3})	1.44	1.45	1.44	1.44	1.45	1.47
Diameter (μm)	12	12	12	12	12	12
Tensile strength (GPa)	2.8	2.8	2.8	3.0	3.4	2.4
Tensile strain to fracture (%)	3.5-4.0	2.8	3.0	4.4	3.3	1.5-1.9
Tensile modulus (GPa)	65	125	101	55	100	147
Moisture regain (%) at 25°C, 65% RH	6	4.3	4.3	-	-	1.5
Coefficient of expansion (10^{-6} K^{-1})	-4.0	-4.9	-	-	-	-

Matrix Material

While most of the attention in a composite material is given to the fiber material, the matrix material is also of importance. While the fiber material is responsible for "carrying the load" associated with composite applications, the matrix material is responsible for many material tasks in its own right. These include positioning fibers as well protecting the fibers from transverse loads buckling, and unfavorable environments.

Matrix materials can be made of ceramic and metal material, however polymer matrix materials are the focus of this research. Although polymers are structurally more complex than metal or ceramic material, they are inexpensive and easily processed, which make them ideal for woven composite impellers. More specifically, the matrix material used in this research is a two component resin and hardener epoxy. This gives to a variety of curing methods including self-hardening, heat-curing, as well as UV-curing.

There are three ways in which matrix material can be applied. The first is a post-process application where large amounts of fibers are initially oriented, and then the matrix material is applied after. This may be favorable for simple composite geometries in that it reduces waste and messes. However, in a post-process matrix application, it may be difficult to distribute matrix material evenly throughout as well as control fiber to matrix ratios. Examples of post-process matrix application can be shown in the impellers in Figure 21 and Figure 22.

Another convenient method of applying matrix material is through the use of pre-impregnated (pre-preg) tows. Pre-preg tows are a bundle of fibers that already contain the epoxy material which is solidified after controlled curing. The hand wound prototype shown in Figure 50 and Figure 52 were made of this pre-preg material. This method is by far the most convenient in terms of eliminating messy resin baths, however it is only available in certain fiber tows. This limits its applicability where specialized fibers and various tow thicknesses are desired. Using a pre-preg tow also limits the custom control of the matrix distribution as well because quantities are pre-determined.

The third and most common method of matrix application is the resin bath or wet winding. This method is practiced by running fiber tows first through a resin bath and then on the mandrel or winding surface. Photos of this method are shown in Figure 20 and Figure 49. Although cumbersome and messy, this matrix application allows for the outright control of distribution on the fiber and can be applied to any geometry.

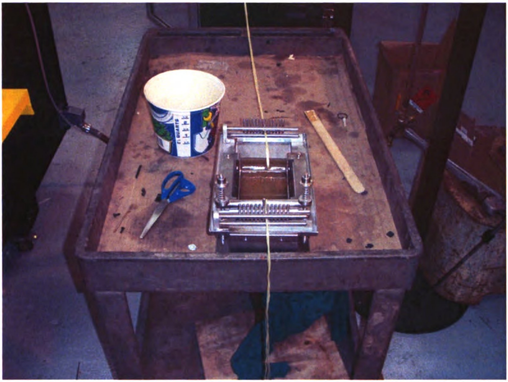

Figure 20. Fiber tow being run through a resin bath for wet winding

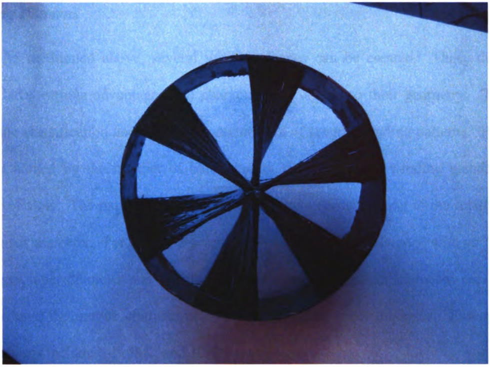

Figure 21. Automatically woven impeller prototype pattern 6-B with post-process applied resin

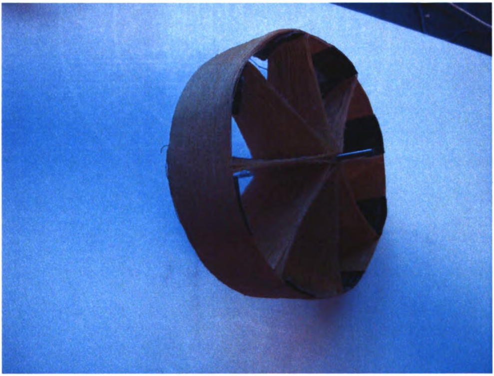

Figure 22. Automatically woven impeller prototype pattern 8-C with post-process applied resin

Winding Patterns

As mentioned above, several winding shapes can be created. These different shapes have various advantages and characteristics unique to their geometry. Table 3 shows the classification and various characteristics of several winding patterns. Patterns are first named by the number of blades, or in the case of the winding mandrel, the number of slots. The patterns are then assigned letters corresponding to the relative size of the inner diameter. Patterns of a given number of blades are assigned with an "A" for the largest inner diameter and "B" for the next size smaller inner diameter, etc. Some patterns have the unique characteristic of having a zero inner diameter. Examples of these patterns include 6-B, 8-C, and 10-D.

Table 3. Abbreviated table of winding patterns (full table in Appendix C)

Number of Points	Pattern	Not Possible	Shape	N	di/do	Notes
5	1, skip 1		5-A			
5	1, skip 2		5-A			Sharp turns
5	2, skip 1		5-A			
5	2, skip 2	x				
5	3, skip 1	x				
5	3, skip 2		5-A			Sharp turns
5	4, skip 1		5-A			
5	4, skip 2		5-A			Sharp turns
6	1, skip 1	x				
6	1, skip 2	x				
6	1, skip 3		6-A	1	0.5	Sharp turns
6	2, skip 1	x				
6	2, skip 2		6-B	0	0	Stack-up in the center
6	2, skip 3	x				
6	3, skip 1		6-A	1	0.5	
6	3, skip 2	x				
6	3, skip 3		6-A	1	0.5	Sharp turns
6	4, skip 1	x				
6	4, skip 2		6-B	0	0	Stack-up in the center
6	4, skip 3	x				
6	5, skip 1		6-A	1	0.5	
6	5, skip 2		6-B	0	0	Solid outside for 3 separate sixths of the circuit, normal inside, stack-up in the center
6	5, skip 3	x				
7	1, skip 1		7-A	1.5	0.62349	
7	1, skip 2		7-B	0.5	0.22252	
7	1, skip 3		7-B	0.5	0.22252	
7	1, skip 4		7-A	1.5	0.62349	Sharp turns
7	2, skip 1		7-A	1.5	0.62349	
7	2, skip 2		7-B	0.5	0.22252	
7	2, skip 3		7-B	0.5	0.22252	
7	2, skip 4	x			0	
7	3, skip 1		7-A	1.5	0.62349	

Shapes:

5-A

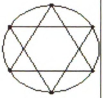

6-A

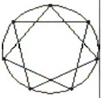

7-A

The second column of Table 3 called "pattern" refers to the repeated winding fiber path. Patterns are in the form, "# skip #". Starting at an arbitrary slot in a winding mandrel, the first number refers to how many slots the fiber must wrap around the outside before entering the slot. For example, if the pattern is "1 skip #", the fiber must start at an arbitrary slot, wrap around the mandrel, and enter the next slot. This is illustrated in Figure 23.

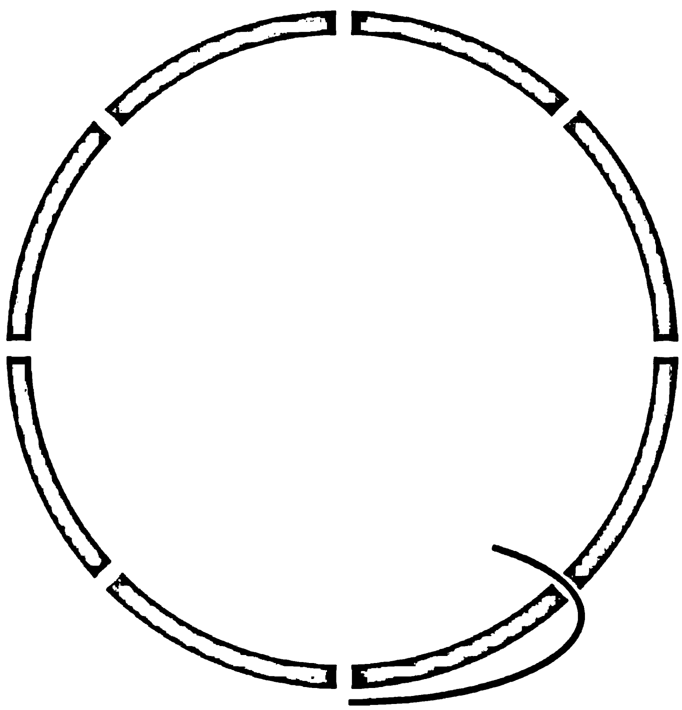

Figure 23. Schematic illustration of fiber path in pattern"1 skip #"

The second number is the pattern refers to how many slots the fiber must skip before exiting through the next slot. For example, if the pattern is "1 skip 2", the fiber must enter the first slot after wrapping around the outside of the mandrel. Then, the fiber must skip 2 slots in the middle of the mandrel before exiting out the next slot to repeat the pattern again. This is illustrated in Figure 24.

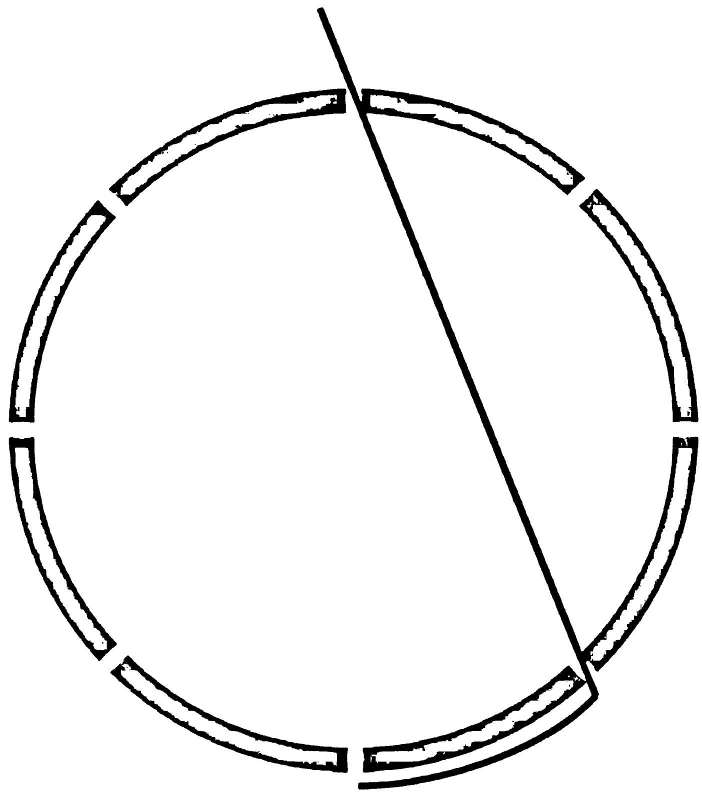

Figure 24. Schematic illustration of fiber path in pattern "1 skip 2"

The ninth column labeled "di/do" is the ratio of the inner diameter to the outer diameter. This is elegantly calculated by Allen Eyler for each shape by the general equation

$$\frac{d_i}{d_o} = \frac{1}{2}\sqrt{\left(1 - \cos\frac{2\pi N}{S}\right)^2 + \left(\sin\frac{2\pi N}{S}\right)^2} \tag{6}$$

where S is the number of slots in the winding mandrel or blades, and N is a pattern factor used in the calculation. This pattern factor starts with zero for patterns that have no inner diameter like 6-B or 8-C. When the pattern has an even number of slots (i.e. when S is an even number) this factor is a whole integer (0, 1, 2, 3,…). When S is an odd number, N is assigned numbers that start at 0.5 and increase by 1 (i.e. 0.5, 1.5, 2.5,…). N factors start at the smallest inner diameter and increase with increasing inner diameter for patterns with the same number of slots. For example, for patterns with 8 slots (i.e. 8-A, 8-B, and 8-C) the *N* factor is 0 for 8-C because it has a zero inner diameter. The *N* factor is 1 for 8-B because it has the next smallest inner diameter, and 2 for 8-A because it has the largest inner diameter for patterns with 8 slots. An example of the *N* factors for odd slotted patterns can be the *S*=7 patterns (i.e. 7-A and 7-B). Here the *N* factor would be 0.5 for 7-B because it has the smallest inner diameter of the 7 slotted patterns. The *N* factor would be 1.5 for 7-A because it has the next largest inner diameter. These are the only patterns for *S*=7. It can be shown that patterns with zero inner diameters are only possible with patterns that have an even number of slots. Therefore, these are the only patterns that may have an *N* factor of zero. This *di/do* ratio is very useful for selecting specific patterns for size constrained applications like hub diameter. It is also useful when selecting various bearing and shaft/axel configurations.

In addition to different size characteristics, the various winding patterns have other characteristics that are worth mentioning. These include fiber paths with sharp turns that may be less favorable for brittle fiber material. Also, some patterns have areas where fibers "stack-up" relative to other areas of the impeller because of frequent overlapping. Characteristics like these are important to identify because they can be advantageous or undesired depending on application.

Advatages of Winding Design

A schematic illustration of a woven impeller can be shown in Figure 25. Here a star shaped configuration is depicted, however virtually any shape can be made. These may include curved blades that increase efficiency. There are several advantages to this design. One is that the woven composite impeller can be mass-produced and rapidly prototyped using a readily available multi-axis winding machine greatly reducing costs. An example such a machine is the McClean Anderson™ Super Hornet® SX9000 shown in Figure 26.

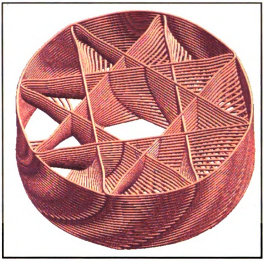

Figure 25. Illustrative model of woven impeller pattern 8-B

By using commercially available software, a design code can be electronically written and carried out by the fully automated winding machine. Utilizing this technology also reduces costs by eliminating the need for additional assembly of components. Various geometries can by constructed by the winding machine including radial-flow and mixed-flow impellers. In addition, the computer design also allows for an outer shroud. An outer shroud adds additional sealing and strength in the tangential direction, thus allowing for an integrated motor at the outer diameter. The star shape depicted in Figure 25 also employs its geometry to segregate the turbulent, separated flow around the hub or inner diameter from the uniform flow along the blades. This flow segregation allows for better efficiency. Structural advantages are discussed in greater detail later in Chapter 9.

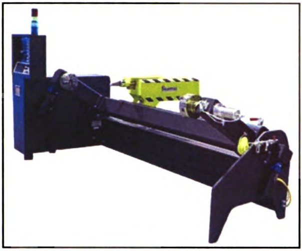

Figure 26. Commercially available Super Hornet winder from www.mccleananderson.com

Driving Scheme

In addition to the geometrical freedoms this impeller offers, the woven or wound impeller also allows for various elegant methods of driving the impeller. Conventional turbo-compressor design employs a separate motor to drive an impeller via a shaft. Although the woven impeller technology can most certainly be used for this driving design, the scope of this thesis includes a more elegant and compact design involving the integration of motor components. By doing this, the compressor impeller in-itself becomes an integral component in the electric motor. Electric motors involve two major components: the stator and rotor. By integrating electrical or magnetizable components in the impeller, the woven impeller can essentially become the rotor portion of the electric motor. The two motor schemes explored in this research are the *brushless* *permanent magnet motor* approach as well as configuration known as an *induction machine* or *induction motor*.

Brushless Permanent Magnet Motor

For simplicity, a permanent magnet motor can be introduced as two electromagnets on a stator surrounding a permanent magnet in its center as the rotor. A schematic illustration of this is shown in Figure 27. Each pair of stator windings make up a motor phase, thus Figure 27 is a single phase motor. A current running through the windings of the stator induces an electromagnetic field that interacts with the permanent magnet rotor. When the similar poles of the permanent magnet rotor, and the electromagnetic stator repel each other, the rotor moves to the opposite poles of the stator. Reversing the current through the stator reverses the poles, and the rotor is repelled again. Repeating this creates a motor torque.

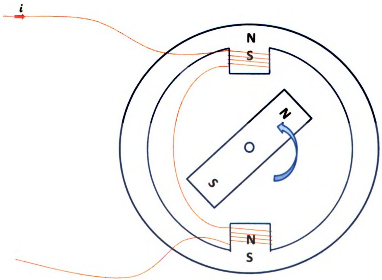

Figure 27. Schematic, illustrative example of a single-phase permanent magnet motor

Although this simple single-phase example is useful for describing the general principle of the permanent magnet motor, it is more common to have several pairs of stator windings. An example of a 3-phase motor is shown in Figure 28. As the number of phases and poles increases, the torque characteristic on the rotor changes as well. An important distinction to make is the mechanical position of the rotor, and the electrical position. The mechanical position θ_m of a rotor is defined by the number of poles facing the air gap N_m, and the electrical position θ_e

$$\theta_e = \frac{N_m}{2}\theta_m \tag{7}$$

So, if a motor with a 4-magnet pole (2-magnet pairs) rotor does one entire electrical rotation, it has only done 180 degrees of mechanical rotation. The electrical frequency f_e and mechanical frequency f_m are related to each other through the number of poles.

$$f_e = N_P f_m \tag{8}$$

Thus, for a certain mechanical rotational speed, the electrical frequency required increases with the number of magnet poles. This is where the motor design is often constrained by the limitations of the input device (frequency converter) that is used to drive the motor. Therefore, fewer magnet poles are used for the design of high-speed motors to keep the electrical frequency down. The drawback for using fewer magnet poles, however, is that the torque production is much lower. The choice of number of magnet poles also ties into the efficiency and overall losses of the design. Since driving the compressor impeller requires high speed and low torque, a motor design with fewer phases is desirable.

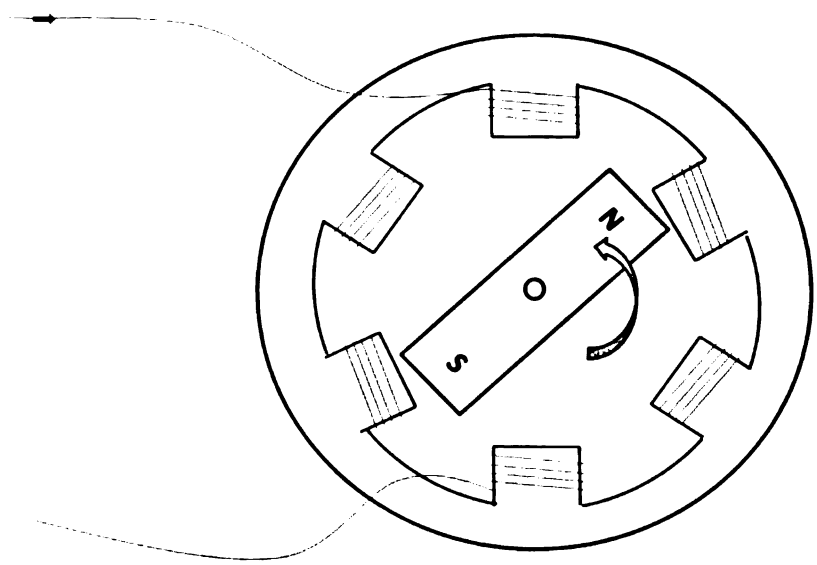

Figure 28. Schematic, illustrative example of a three-phase permanent magnet motor

This type of electric motor concept can be integrated into the woven composite impeller by introducing magnetic material to the wheel. This may be done by attaching magnets to the outer shroud of the impeller or by magnetizing the impeller material itself. One interesting method of magnetizing the woven impeller is by introducing a material into the resin during winding that is either magnetic itself or has the ability to be magnetized. This includes the use of various iron compounds and mixing them within the resin.

Induction Motor

Another option for an integrated motor is the use of an induction machine. This motor configuration is an attractive option for initial experimentation because of its ease of manufacture. In an induction machine, AC power is used to "induce" electromagnetic fields that are out of phase with one another and essentially "magnetize" a conductive rotor. Because of this, the rotor need not have permanent magnets, but only be made of conductive material. Since the rotor only needs to be constructed of conductive material, the integrated woven impeller does not need to be magnetized, nor have magnets placed within the impeller. This is advantageous because integrating magnets and magnetizing the impeller can be a difficult task, especially in the initial demonstrations of feasibility.

The easiest design for an integrated induction machine is simply to wind the impeller on a mandrel that is made of conductive material and not remove it. The impeller and mandrel can then be placed in an electric stator designed for induction machines. A picture of this configuration can be shown in both Figure 67 and Figure 68. Different bearing configurations are also possible and will later be discussed in Chapter 10.

Although the ease of manufacture makes this integrated motor option very attractive, it is not without its own inherent challenges. One of these challenges is that it requires a 3-phase power supply, which although available in many laboratories and industrial settings, is not readily available in a residential setting. Induction machines also require small air-gaps in between stator and rotor which makes for tight machining tolerances.

CHAPTER 9 : COMPUTATIONAL ANALYSIS OF DESIGN

Pattern Modeling

To generate accurate computer models of the winding patterns classified in Chapter 8, a computer code was written in C++ by lab member, Allen Eyler [26]. This code could generate several outputs automatically that could be directly used in applications such as: 3-D modeling software like Unigraphics™, matrix simulation, winding mandrel design, as well as the accommodation for material variation. This code was also employed for physical rapid prototype generation as well as computational structural analysis and preliminary simulations in computational fluid dynamics.

Interfacing for 3-D Modeling

In addition to a series of points Eyler's code generated, it also outputted GRIP (Graphics Interactive Programming) commands. GRIP commands are an interface language supplied by Unigraphics™ to generate 3-D models. They specify the arcs, lines, surfaces, splines, and support mandrel of any winding pattern. Manual inputs and code execution took less than 2 minutes to complete the 3-D models like the one shown in Figure 29. Here we see a 3-D model of pattern 8-2-2 including its support mandrel.

Radius of Curvature around Slots

The program is sophisticated in that it not only models the winding pattern shapes, but also models the actual fiber paths and behaviors as they are constructed. The computer code calculates and specifies the lines, arcs, and even the radius of curvature as the fiber wraps around and through the mandrel slots. Figure 30 illustrates this specified radius of curvature.

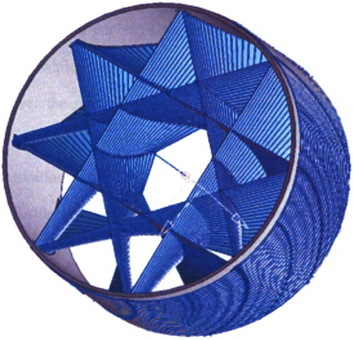

Figure 29. Computer model of woven impeller including its support mandrel

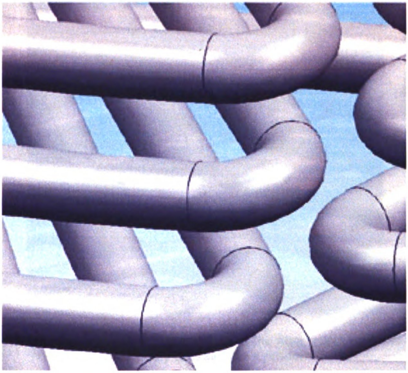

Figure 30. Magnified detail of a wound impeller model, illustrating the radius of curvature of the fiber

Fiber Collisions

In addition to the radius of curvature, the model also elegantly takes into account fiber collisions. In reality, while winding a fiber across the middle of the mandrel, a fiber would come up and over the previously placed fiber below it. However, computer modeling avoids these collisions by defining separate line segments that fibers follow to overlap nicely. An illustration of these defined lines segments and fiber overlapping can be shown in Figure 31. Although these fiber collisions are not much of an effect on some patterns, other patterns such as 6-2-2-B shown in Figure 32 have fibers that all cross the center of the impeller. This makes for a large accumulation of fibers stacking up in the middle that the model needs to account for.

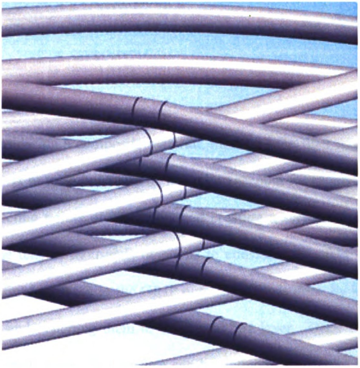

Figure 31. Detail showing collision avoidance of the fiber with segments that have previously crossed the cylinder

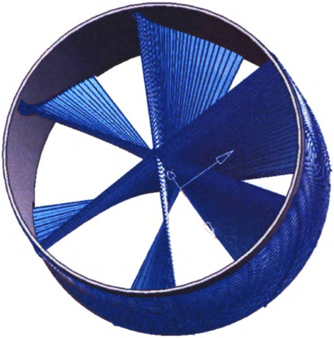

Figure 32. An Impeller Model in which all fiber collisions occur at the center of the cylinder

Modeling the Resin

When considering a composite material, modeling the fiber material is only half the task. The matrix or resin must also be taken into account for accurate modeling. This is done by connecting points on the fibers and creating a surface. This can be tedious since there can be tens of thousands of points to consider. For this, the original code must generate defined surfaces in the GRIP outputs. This is done by locating endpoints of line segments and matching them to their specified layer. Once enough points and layers are determined, a specified surface can be defined. Repeating this for the entire impeller defines all surfaces on the woven wheel. These surfaces serve to model the resin applied during the actual wheel manufacturing.

Structural Analysis

Recall from Chapter 4 that to achieve the necessary pressure ratios to employ the use of water as a refrigerant, very high tip speeds must be achieved. Also recall that the majority of the forces on the impeller are from its own inherent mass rotating at high speeds. Because of this, computational simulations must be analyzed to assure the woven impellers withstand these high speeds. These simulations were completed and analyzed by lab member, Anirban Lahiri [27] using FEM (Finite Element Method) along with ANSYS™ software.

Setting up the Simulation

The material properties used in the simulation were from the Kevlar® 49 properties tabulated in Table 2. Rotational speeds were ramped up to 120,000 RPM to simulate motor startup and operation. To set-up the meshing of the geometry, Eyler's code [26] was again employed to be used in a MATLAB® code to then generate an ANSYS™ log file. The geometry was then specified and a mesh could be applied. The meshing used in this analysis was Quad 8 node 82 element. This is a quadratic element and provides a better accuracy than its corresponding linear element. It is also an appropriate element for a plane stress analysis. The geometry can be map meshed too, however a free meshing provides pretty good elements with almost zero distorted elements. Stresses and displacements were analyzed while varying parameters such as skip number and fiber thickness.

Simulation Results

The displacements and stresses were determined and plotted. A small sample of these plots is shown in Figure 33 through Figure 40 below. The following figures determine a general nature or trend of various winding patterns. It is very important to note that the **displacements conveyed in the figures were greatly exaggerated for detection purposes within each individual pattern**, and that the actual displacements are much smaller in reality. It should also be noted that the scales of each plot are greatly different as well. The plots are to observe the relative displacements of locations within each pattern themselves.

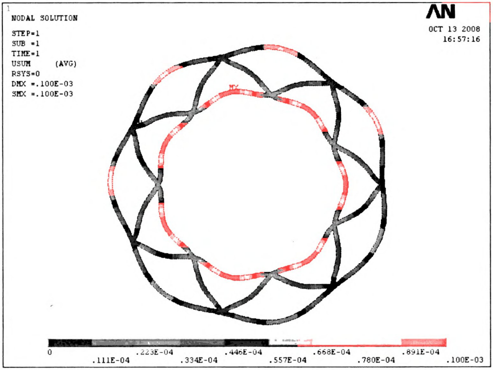

Figure 33. Pattern 7A - Displacement

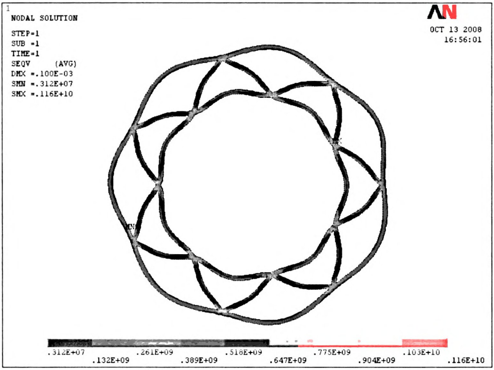

Figure 34. Pattern 7A - Stress

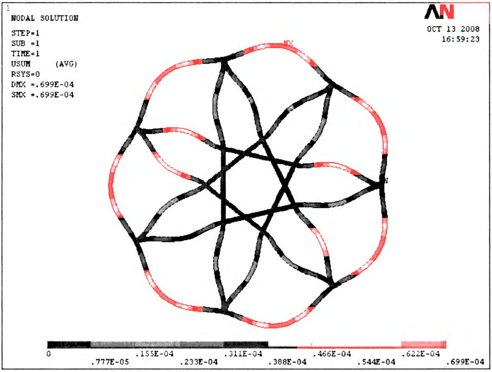

Figure 35. Pattern 7B - Displacement

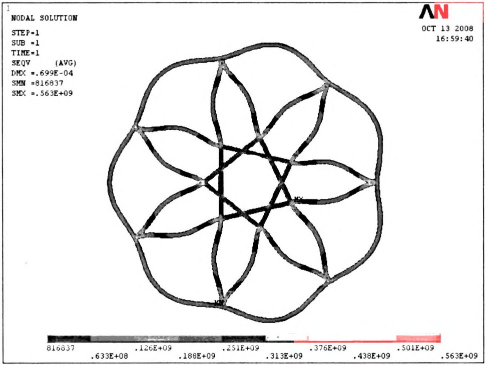

Figure 36. Pattern 7B - Stress

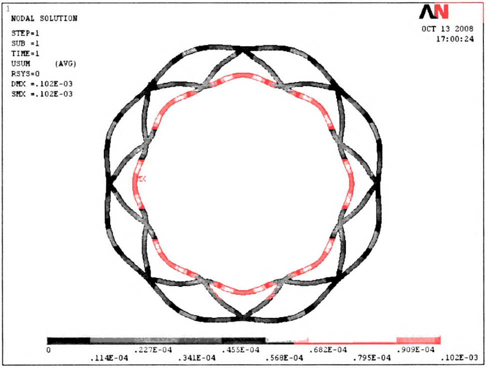

Figure 37. Pattern 8A - Displacement

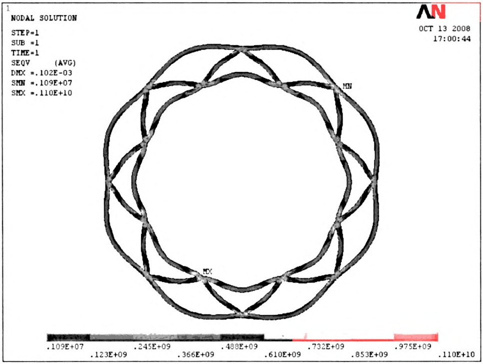

Figure 38. Pattern 8A - Stress

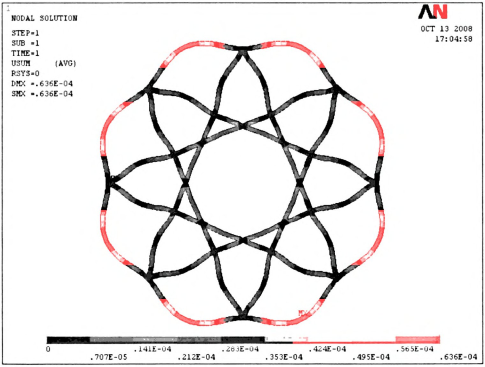

Figure 39. Pattern 8B - Displacement

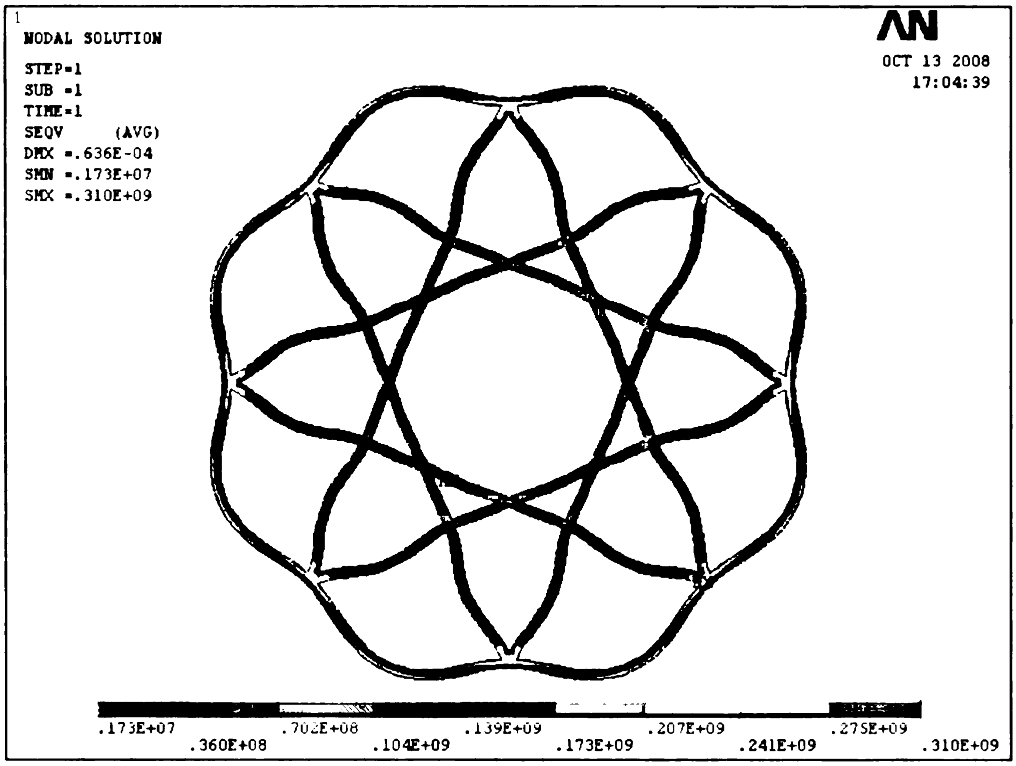

Figure 40. Pattern 8B - Stress

Analysis of Simulation Results

An interesting observation from the displacement diagrams is that for the A types of designs, the maximum displacements occur in the inner fibers while they occur in the outer fibers for every other design styles like B,C, D, E, etc. Also, another observation is that as the inner circle becomes smaller (as the number of skip increases), the stresses in the inner fiber decreases. This can be explained from the simulations in the varying thickness outer shroud simulations. So as the fibers pass through the centre, the stresses become less.

Effect of Skip

Recall from Chapter 8 the winding patterns included a skip number that denotes the number of slots the fiber "skips" before it exits the mandrel. One can make the generalization that the higher the skip number, the smaller the inner hub area of the impeller is. The skips were varied for the different impellers and the stresses were studied. Simulations were done until the number of points on the circumference of the impeller was 24. The results plotted in Figure 41 through Figure 43 below indicated that the stresses reduced as the number of skips increased. For convenience, the skip numbers are divided into low (6-9), medium (10-14) and high (15 and above). The stresses decrease monotonically as the number of skips increase. It can also be shown that the stresses flatten out and do not increase or decrease very profoundly after skip 2.

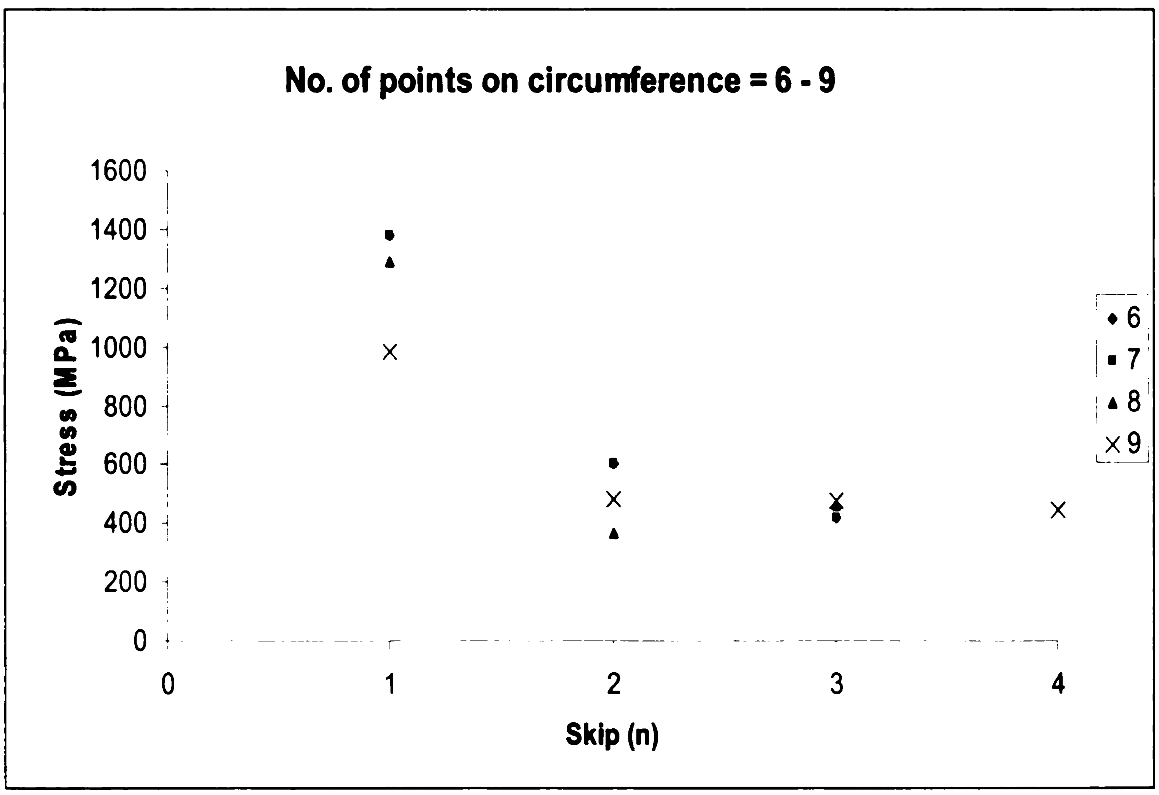

Figure 41. Stress vs. skip for patterns with 6-9 slots

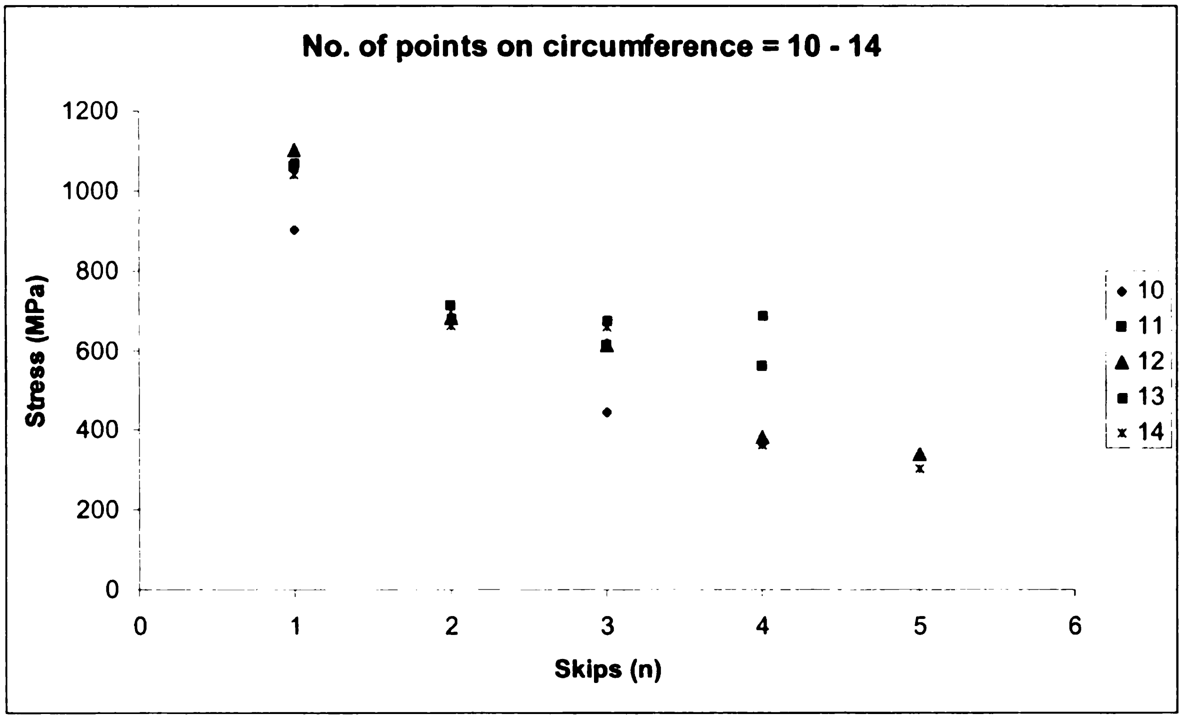

Figure 42. Stress vs. skip for patterns with 10-14 slots

For the 10 through 14 patterns, the maximum skips are 5. Again, the stresses show the same behavior as in the 6 through 9 patterns. The last case shown here is the case where the numbers of points on the impeller are from 15 to 18. Almost all of the points show similar behavior as the cases shown in Figure 41 and Figure 42. However, as the skip is increased, or patterns like 18 and 19, the stress does not monotonically increase or decrease with skip. This may be due to the fibers getting close to each other and having non linear interaction effects.

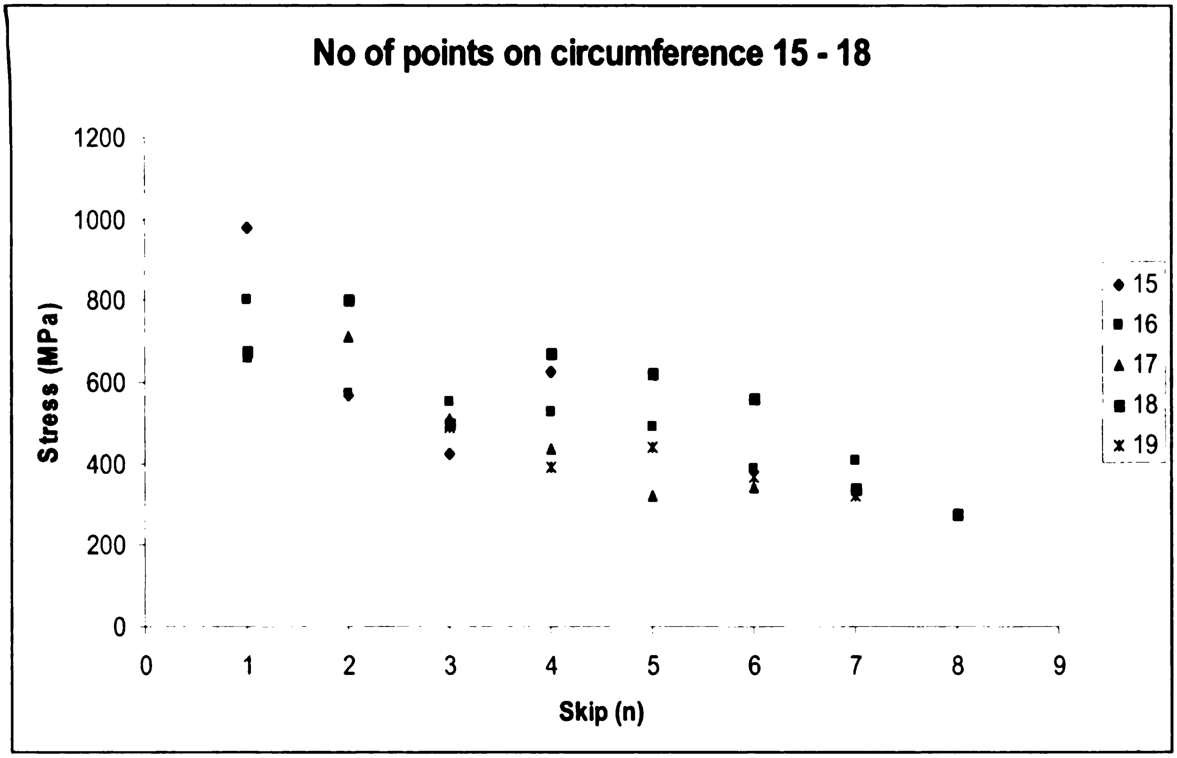

Figure 43. Stress vs. skip for patterns with 15-18 slots

Effect of Fiber Thickness

In plotting the effect of varying fiber thickness, the results were again documented with reference to the number of slots in the winding patterns. Fiber thicknesses of both the blades and the outer shroud of the impeller structure were selected as 1 and 2mm. All the thickness simulations are not shown here because of space issues. However, the general behaviors of the curves are the same.

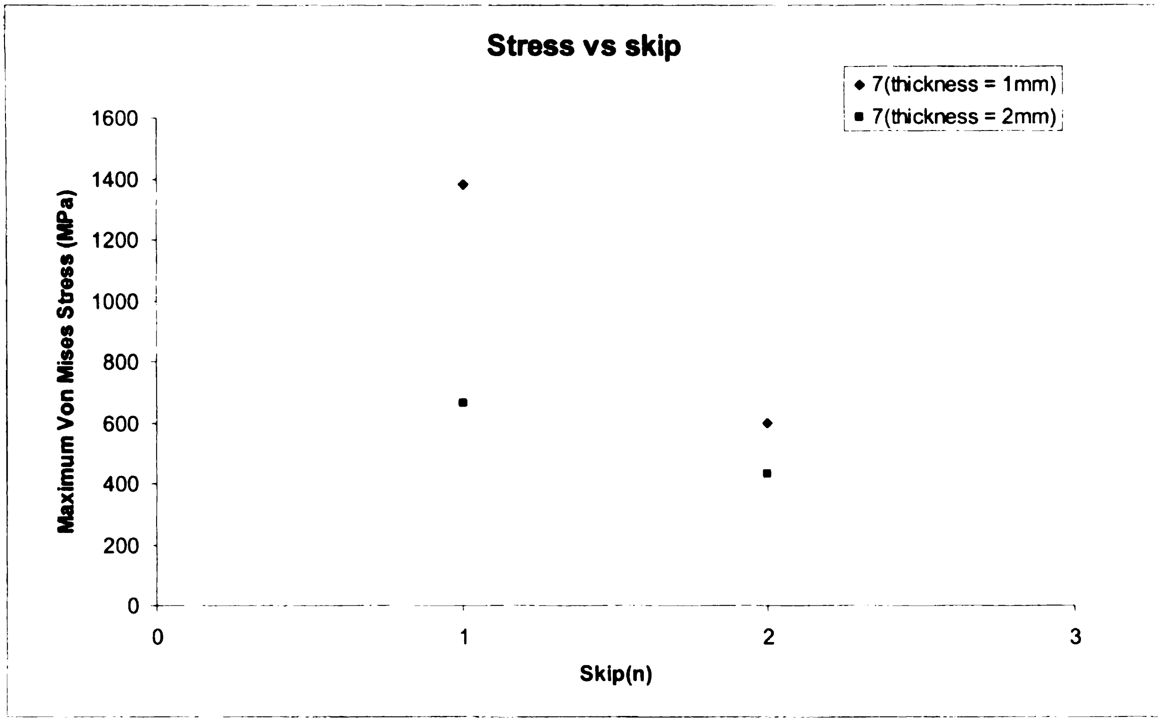

Figure 44. Effect of fiber thickness for 7 slot pattern

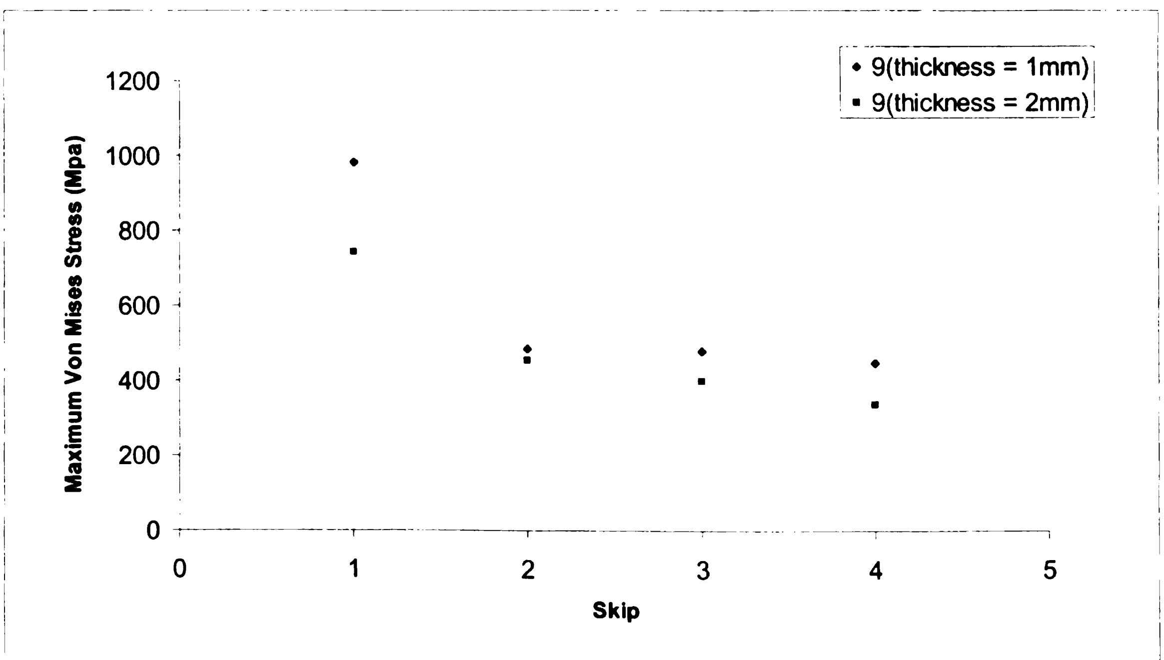

Figure 45. Effect of fiber thickness for 9 slot pattern

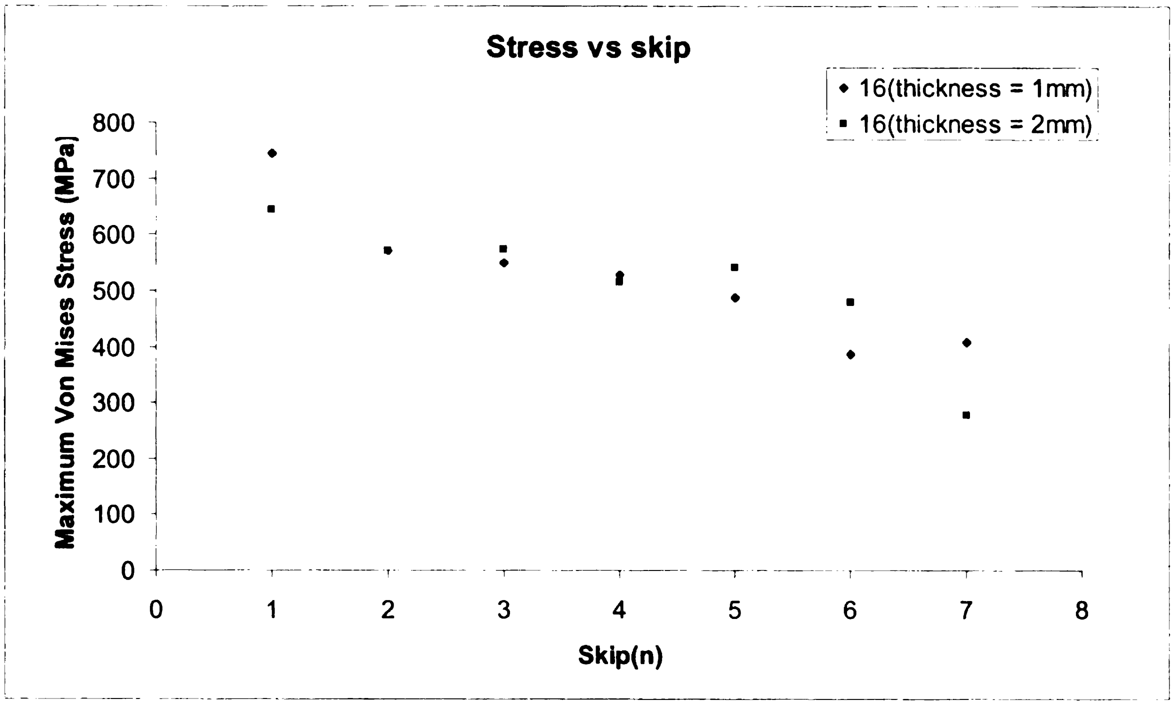

Figure 46. Effect of fiber thickness for 16 slot pattern

Figure 44, Figure 45, and Figure 46 show that the stresses decrease as the thickness of the fibers are increased. In order to explain this phenomenon, two cases have to be considered. The first one is based on the variation of stresses in an annulus by changing the inner diameter. As can be shown from the Figure 32, the tangential stress is the predominant stress component when the annulus is subjected to a rotation. The total stresses (vector addition of the radial and tangential stress) follows more or less along the lines of the tangential stress. It can be shown that as the annulus is made thicker, the total stresses decrease in the annulus. The decrease of stresses in the different patterns can be attributed to this. Also, there is a pull on the outer shroud by the blades, which is more as the thickness is increased, leading to less stresses in localized areas.

Thus, in conclusion, thickness plays an important role in the determination of stresses in the fibers. Clearly, a low thickness is desirable for lower stresses, however, during the manufacturing process, the actual thickness of the fibers manufactured are pretty low (around 1mm). Even when coated with resin, the thickness does not increase a whole lot. An alternative to this is the stacking of fibers together in the force direction to reduce the stresses. Also, an increased fiber concentration at the areas where the stresses are highest may help in reducing the stresses.

Rapid Prototype

The first physical models of the woven impellers were created on a rapid prototype machine. Using the Unigraphics™ file, the machine can create physical prototypes by arranging thin layers of plastic or 3-D printing. An example of one of these models is shown in Figure 47. Here a woven impeller with a central hub is shown with its electrical stator.

Figure 47. Rapid prototype of woven impeller with electric stator

Hand Winding

The simplest construction of a woven impeller is one wound by hand. Although the automated manufacturing of the impeller is one of the most important advantages of this design, initial prototypes were constructed simply by winding Kevlar thread around the mandrel. This hand winding can be shown in Figure 48, Figure 49, and Figure 50.

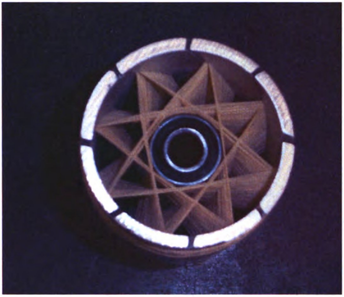

Figure 48. Dry hand-wound prototype to be used in integrated motor

The initial hand winding was done with dry fiber to obtain a prototype demonstrating the pattern design. This dry winding is shown in Figure 48. In addition to the pattern model, this prototype was also used in an integrated motor demonstration discussed later. The wet winding method where dry fiber tows are guided through a resin bath is shown in Figure 49 and its finished winding pattern is shown in Figure 51. The resin for this prototype was cured at room temperature using a self-hardening resin. Hand winding using a pre-preg tow is shown in Figure 50, as well as its finished result before curing in Figure 52. This model was heat-cured in an oven and its mandrel removed.

Figure 49. Hand winding using dry fiber and resin bath

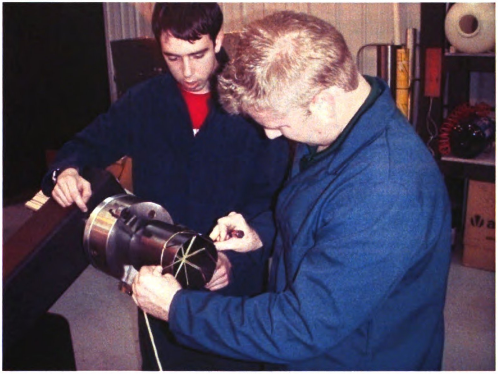

Figure 50. Hand winding using pre-preg fiber

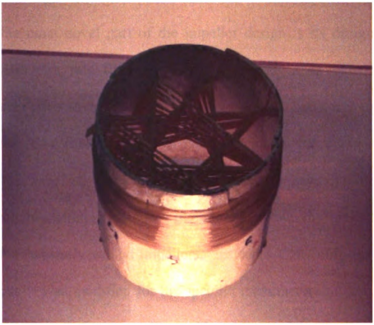

Figure 51. Finished result of hand winding using resin bath

Figure 52. Finished result of pre-preg hand winding before heat curing

Automated Winding

Perhaps the most novel part of the impeller design is its design for automated manufacture. Although this filament winding method is an existing and proven technology for other parts such as pressure vessels and golf shafts, it is to the knowledge of the author that this method has not been employed for compressor impellers. Moreover, for the sake of convenience as well as to save additional costs, the commercially available winding machines like the one shown in Figure 26 was not used to create initial mechanically wound impellers. Instead a CNC mill that was purchased from CNC Masters™ was modified for the specific manufacture of compressor wheels. A photo of this set-up can be shown in Figure 53 and Figure 54. The main reason for this decision was that the CNC mill was approximately 10 times less expensive than purchasing a winding machine. In addition to this, the mill could also be used to manufacture mandrels as well as other mill duties that arise in the turbomachinery laboratory at Michigan State.

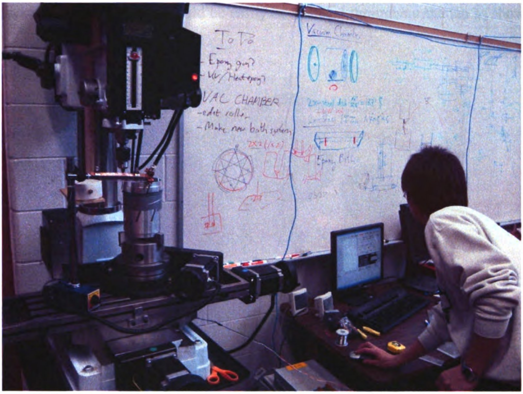

Figure 53. Photo of CNC winding set-up

Modifying the CNC Mill

To modify the CNC mill for winding impellers, several additions had to be made. The first was to simply make the machine portable throughout the lab. The CNC mill came as a small table-top mill with an optional stand to be mounted to a shop floor. Since the stand was designed to be attached to the floor, it was made of light-weight material. To make the mill portable throughout the lab, caster-wheels were required to be installed on the bottom of the stand. The lightweight stand beneath the heavy mill made the machine top-heavy and prone to tipping. To alleviate this, a large, heavy slab of steal was attached to the bottom of the stand and caster-wheels installed. The result was a sturdy, versatile machine that could be easily be wheeled throughout the lab as shown in Figure 54.

Figure 54. Portable CNC winding machine

The CNC stage itself needed no modification. An add-on turn-table axis was purchased from CNC Masters™ and along with the x-y-z stage and the spindle, the mill provided a 5 axis CNC stage. A spool was installed to mounts on the side of the machine along with a container for a resin bath, including guiding rollers for filament winding. These modifications are shown in Figure 55.

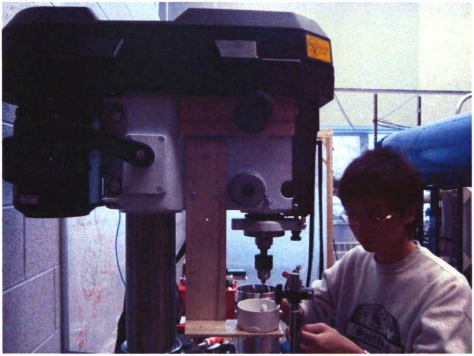

Figure 55. Winding machine with fiber spool and resin bath added

Next, the fiber thread needed to be guided throughout the mandrel in various winding patterns. This was done using a sewing machine type needle also referred to as the leader. Although the basic idea of leader method remains the same, it has had several improvements. The initial leader was made of small copper pipe. The pipe was secured in the spindle's chuck, a hole was cut into the side for the thread to enter, and the thread was then lead out the bottom end of the pipe to be guided around the mandrel. Although this method served as a good initial attempt, it lacked in accuracy because of the freedom of the thread to move laterally within the copper pipe. The leader has evolved into a more accurate tool by using a very thin tube, bending it to the angle of the mandrel slots and securing it again to the spindle's chuck. This tooling method is shown in Figure 56.

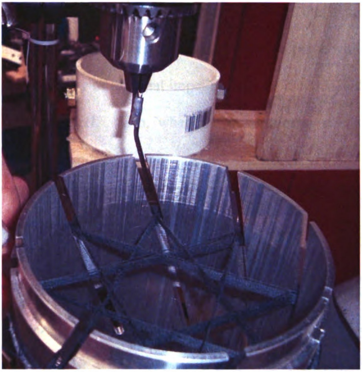

Figure 56. Photo of winding with leader tool

Challenge of Fiber Creep

One of the challenges that arouse from the initial attempts at automated winding was the phenomenon that was named fiber creep. This occurred mainly during dry winding attempts. When the fiber thread was guided around the outside of the mandrel and the leader was raised up and over the side of the mandrel, the previously laid fiber tended to "creep" up the side.

One cause of this fiber creep was the lack of friction between the outside of the mandrel and the fiber thread. This was especially prominent during dry winding attempts without the resin because the resin causes the thread to "stick" to the mandrel. The initial method to address this challenge was by attaching a high-friction material to the outside of the mandrel. This high friction material came in the form of sandpaper. As shown in

Figure 57, sandpaper strips were attached to the outside of the mandrel prior to dry winding. Although this method worked to keep the fibers in place while winding, it did negatively affect the geometry of the final impeller because it added additional thickness in some areas of the mandrel. Also, when the post-process resin was applied, the sandpaper was difficult to remove.

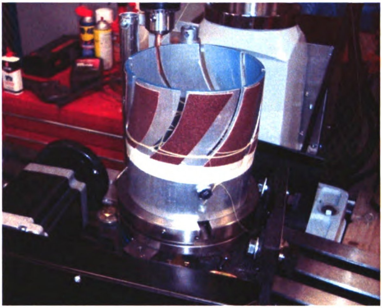

Figure 57. Sandpaper applied to outside of mandrel for added friction

In addition to applying a high-friction material to keep the fibers in place, another solution was explored to re-position the fibers if they crept up. To do this, an electronic actuator was placed on the outside of mandrel that would "poke" the fibers back into position at a time-controlled rate. Although fiber creep reduces significantly while wet-winding, it is still a phenomenon that needs additional observation.

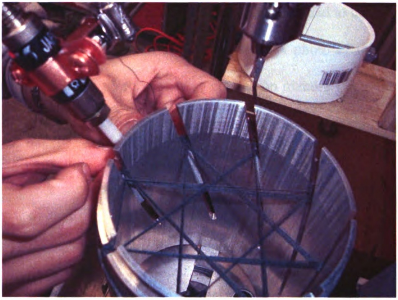

Figure 58. Winding shown with actuator to re-position fibers after fiber creep

Another cause of fiber creep is the tension created by the leader itself. With limited to no tension control, cases arise when the tension is so large that the leader "pulls" the fiber up and away from its intended position on the outside of the mandrel. Tension control is a major factor in creating any accurate filament wound structure [28]. To enhance fiber placement, a tension control method is being researched. This may include force transducers, torque controlled motors on the fiber spool, or even friction material in the rollers or spool.

The Patterns

Since several of the hand wound and rapid prototype models were constructed in the 8B pattern, the initial automated windings were also done using this pattern and an example of this can be shown in Figure 59. However, two patterns were wound that had no inner diameter as described in Chapter 8. These were patterns 8C and 6B. To fix a small shaft to the center of these patterns, a shat was positioned in the center of the pattern while the winding was completed. The winding code had to take this into account by leading the thread slightly around the small shaft. A photo of this winding can be shown in Figure 60. Several prototypes were created on mandrels of 5 inch diameter, as well as with mandrels with 2.375 inch diameter.

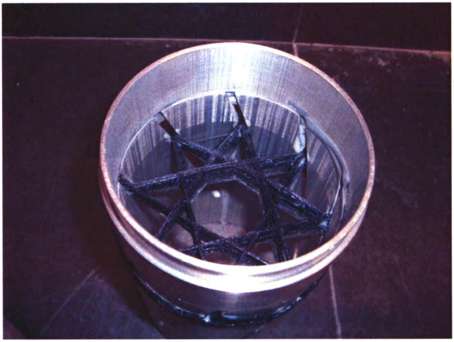

Figure 59. Automated, wet wound prototype of pattern 8-B

Structu

during

structur

high sp

compre

must b

velociti

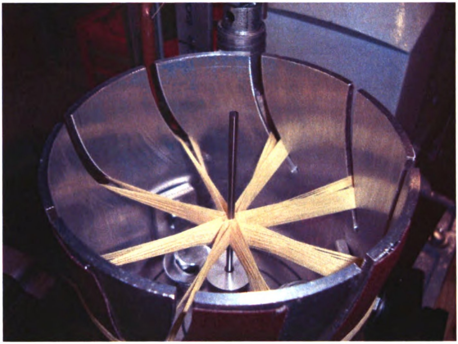

Figure 60. Winding pattern 8C including a shaft

Structural Spin Test

To demonstrate that the woven impeller prototypes can withstand the forces during operation, a structural spin test was performed. The initial challenge of a structural spin test is obtaining a mechanical drive to spin the prototype impeller at very high speeds. As mentioned, the primary motivation of this research is to effectively compress water vapor for mechanical refrigeration. To achieve this, very high tip speeds must be attained. These tip speeds are in excess of 350 m/s. Rotational or angular velocities are related to tip speeds by the equation

$$\omega = \frac{v}{r} \qquad (9)$$

Where ω is the angular velocity in radians per second, v is the tip speed or circumferential velocity, and r is the radius of the impeller. Most drives have speeds rated in terms of revolutions per minute or RPM. Angular velocities in rad/s can be written in terms of RPM by the equation

$$n = \omega \frac{30}{\pi} \tag{10}$$

Where n is the rotational velocity in RPM. From these equations,(9) and (10), one can find the rotational speed of the drive needed to reach 350 m/s for a given impeller radius. As mentioned above in the *Mechanical Winding* section of this chapter, the larger impellers were 5 inch diameter. For this radius, a drive must spin the wheel at 52,634RPM to achieve 350 m/s tip speed.

Table 4. Spin test inquiries and quotes

Company	Quoted work	Cost
BALCO	Perform dynamic balancing and spin/burst testing on one piece	$2500
Test Devices Inc.	Conduct spin test with engineering consultation	$20,000
Hines Industries	Obtain dynamic balancer or conduct balancing test. Suggested a static toy plane prop balancer	No quote
Hi-Tek Balancing	Company only does balancing	No quote
Walter Gear Drives	Obtain a speed increasing gearbox rated 50,000-90,000 RPM	$50,000
Barbour Stockwell	Obtaining test equipment	$500,000

For the given budget of this project, this is easier said than done. While many high speed drives exist as well as companies who conduct structural spin tests, this hardware and services are extremely expensive as outlined in Table 4. To address this issue, several methods of a high speed spin test are currently being investigated. However, data for only one method has been collected so far.

High-speed Air-turbine Grinding Tool

One relatively inexpensive method of driving the woven impeller is with a high-speed air-turbine grinding tool. An air-turbine tool was purchased for \$473.77 and was rated at 65,000 RPM with a power rating of 0.5 hp. The tool was mounted in a test stand and surrounded with plexi-glass and wire mesh for safety in the event of a structural failure. Pictures of this set up can be shown in Figure 61 and Figure 62

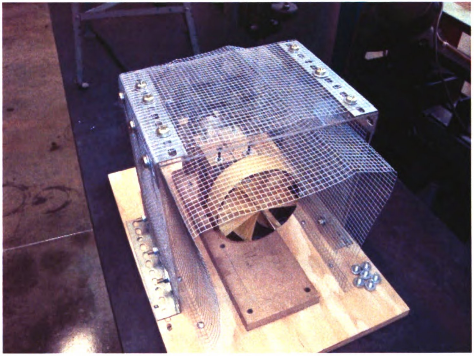

Figure 61. Photo of spin test using air-turbine (front view)

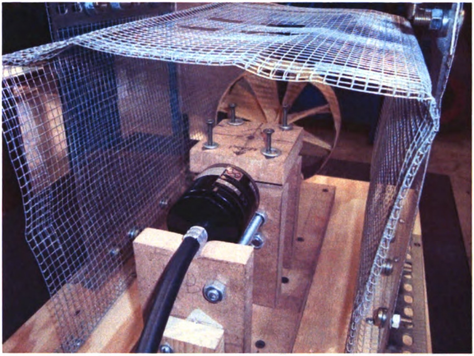

Figure 62. Photo of spin test using air-turbine (rear view)

When the tool was tested with no load using the compressed air-line available in the turbomachinery laboratory at MSU, rotational speeds of 57,000 RPM were confirmed using an optical tachometer. However, when the woven wheel was coupled to the tool, speeds of only around 4,000 RPM were reached as shown from trials 1 and 2 from Table 5.

Balancing and Vacuum

From the vibrations and air flow of the first trials of the spin test, the need for balancing and vacuum were evident. Balancing is an important challenge in the design of any rotating machinery as unbalances can be attributed to power losses as well as mechanical failure. To combat this, a flexible shaft was coupled to the shaft. This is shown in the left photo of Figure 63. In addition to the flexible shaft, a static balancing of the test impeller was conducted. Impeller imbalances were identified and alleviated by adding additional resin, or in some cases lead tape to light areas of the impeller. A photo of this balancing can be shown in the right photo of Figure 63. Although the shaft and static balancing did alleviate some of the vibrations, it did not greatly change the speed reached by the impeller driven by the air-turbine.

Figure 63. Flexible shaft coupled to wheel (left) and static balancer (right)

To reduce impeller work, a clear plastic food container was placed around the impeller, as shown in Figure 64. This reduced the airflow created by the impeller and hence the work done by the impeller. This did increase the effectiveness of the air-turbine test as shown by the later trials in Table 5. A top speed of 6,518 RPM was achieved at which the impeller structurally withheld. At this point it was concluded that the air-turbine did not have the sufficient power, as it was rated, to rotate the woven impeller at high the speeds for a structural spin test.

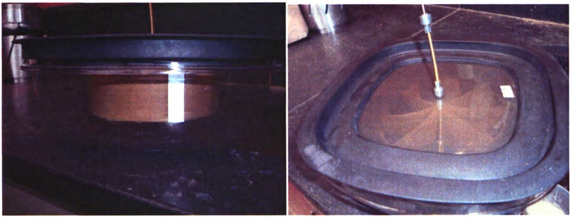

Figure 64. Airflow prevention chamber for spin test

As noted before and shown in Figure 64, blocking the airflow with a plastic container gave way to larger speeds. This was achieved by reducing the work done on the air by the impeller. To eliminate this work completely, and therefore increasing the effectiveness of the drive even more, a vacuum chamber must be employed. A schematic illustration of such a vacuum test chamber can be shown in Figure 65.

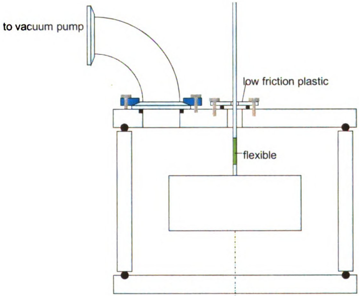

Figure 65. Design illustration of vacuum test chamber

Table 5. Air-turbine spin test trials

Trial	Maximum Speed Reached (RPM)	Structurally withheld?
1	3403	Yes
2	4812	Yes
3	5140	Yes
4	5211	Yes
5	6529	Yes
6	6518	Yes

RC Racecar Nitro-motor

Another method of driving the woven impeller in a structural spin test is by the use of a radio controlled racecar engine. These little engines are relatively inexpensive and advertise high speeds and power. To confirm these claims an engine was purchased from Larry's Performance RC's in Sterling Heights, Michigan. The name of the model is the Ax 28 Spec 1 and the manufacturer advertises that it can reach speeds of 34000 RPM and that it is rated at 1.157 hp. A test bench was also purchased from a local hobby shop to break-in and max out the engine. A preliminary test set-up of this experiment is shown in Figure 66. This test is currently being conducted.

Figure 66. Test bench for RC racecar nitro motor

High-speed Router Tool

Also being currently performed, is a spin test using high-speed router tools. Two routers were obtained from www.cpooutlets.com. One is a Bosch PR20EVSK and is rated for speeds up to 35,000 RPM and a power of 1 hp. The other is a Milwaukee 5625-20 and is rated for speeds up to 22,000 RPM and power of 3.5 hp. It is envisioned that the drives in these routers can be coupled to a woven impeller in a test stand to perform a structural spin test.

Integrated Motor

As mentioned in Chapter 8, one of the most novel aspects of the presented technology is the integration of a motor into the woven impeller design itself. Preliminary realizations of two configurations were conducted.

Induction Motor

Chapter 8 presents the simplicity of designing an induction machine to be integrated with the woven impeller. To carry out physical models of this design, several induction motors were either purchased or generously donated to MSU by Lansing Electric Motors, Inc. These motors were taken apart and their rotors removed. The inner diameters of the motor stators were measured, and mandrels were created to fit within them with somewhat generous clearance for proof of concept. To create an integrated motor using this configuration, the mandrel needed only to be made of conductive material. For its electrical conductivity and its ease of machining, aluminum was selected to machine the mandrels. Two woven impellers were wound and configured to spin in the electrical stators with two different bearing configurations.

The first configuration was done using a shaft and bearings that fit the motor housing. This configuration can be shown in Figure 67. This motor housing was useful because it was already fitted for commercially available bearings and fitted concentric with the center of the stator. This eliminated the need for manufacturing axel struts or supports that had to be made concentric with both the motor-stator and shaft. The electric stator was connected to an AC frequency inverter that could change the frequency of the electrical current supplied by the laboratory. The inverter drives the woven impeller by its integrated motor in this configuration at 6,000 RPM and structurally withheld.

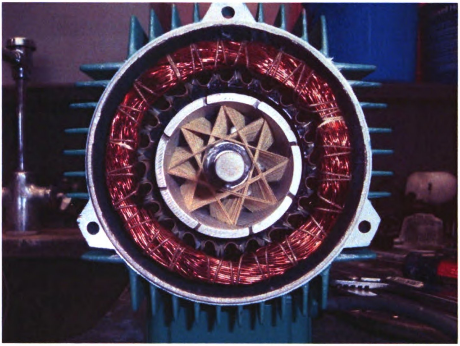

Figure 67. Prototype woven impeller with integrated motor in an induction machine

The second bearing configuration was constructed using a larger mandrel that was professionally machined out-of-house. This mandrel was machined with a slightly smaller outer diameter at the ends than the rest of the piece as shown in Figure 56, Figure 59, and Figure 68. This was done to fit plates that acted as bearings at the ends of the motor stator as shown in Figure 69. Low friction plastic called Delrin® was also fitted to the outside of the aluminum mandrel shown in Figure 69. This woven impeller was driven by its electric stator at 10,000 RPM and also structurally withheld.

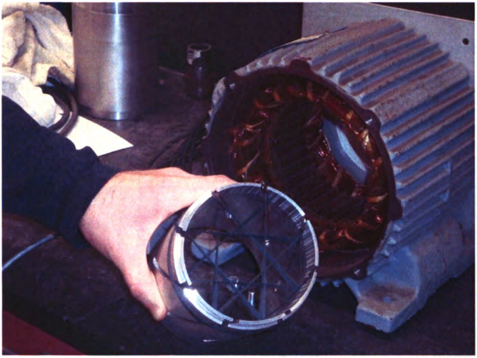

Figure 68. Woven impeller shown with its corresponding electromagnetic stator

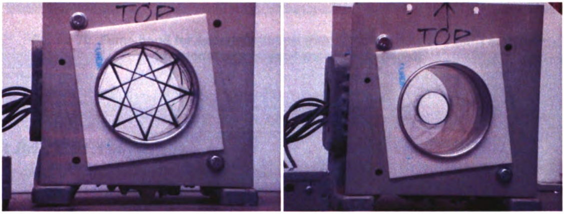

Figure 69. Woven impeller with its integrated motor shown still (left) and spinning (right)

Permanent Magnet Motor

To realize the design of an integrated motor using a permanent magnet approach, initial experiments have been conducted using iron powder and the epoxy resin. Because of the hazardous effects of inhaling air-borne iron particles, a fume hood has been created and installed in the laboratory and can be shown in Figure 70 (left). Initial experiments using magnets shown in Figure 70 (right) indicate that an iron powder mixed with an epoxy resin has the potential to be magnetized and thus used in a permanent magnet motor configuration.

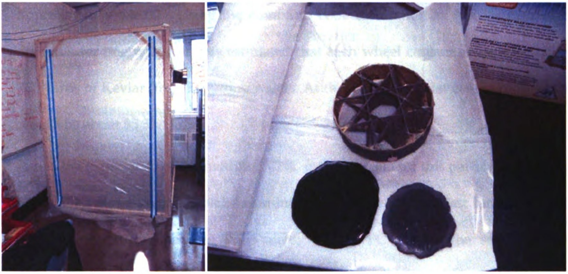

Figure 70. Fume hood for experimentation with magnetic powders (left) and iron-powder/epoxy mixture experiments (right)

A Brief Cost Analysis

High performance impellers used in current water vapor chillers have been priced at roughly $50,000 per wheel [16]. As mentioned in Chapter 6, Current State of the Art, this is a common reason that hinders the application of R718 units in the US. A brief cost analysis has been performed to demonstrate the economic advantages of a compressor using a woven composite impeller.

- For the cost analysis of the woven impeller the "consumed" materials were the resin and Kevlar fiber. Taking into account the cost of resin needed for each wheel, plus taking into account some waste losses or "scrap", it is estimated that each wheel takes approximately 60 mL of equal parts resin and hardener. Both resin and hardener were purchased at about $30 per liter. Hence the resin or matrix part attributed to each wheel was about $1.80.

- For the Kevlar portion of the wheel, the cost of a 6,000 yard spool of Kevlar was approximately $46.00. Using the computer code calculation as well as measured amounts for one wheel, it was estimated that each wheel consumes approximately 700 yards of Kevlar fiber, including waste. At this rate the Kevlar cost of each wheel would be about $5.37.
- A real life expectancy of the modified CNC machine used for this particular winding application is not yet available. Assuming conservatively that it last for about 8,000 wheels. Since the machine itself along with a PC to run the software cost approximately $9,000, the working hardware for each wheel would be $1.13.
- Since the system is fully automated, it is estimated that a technician could be trained to oversee the manufacture of the impellers on average about 1 hour per 20 wheels. At a rate of $50 per hour, the labor cost of each wheel would be about $2.50 per wheel.
- The concluding cost of each wheel would then be $10.80. This is extraordinarily less than the $50,000 cost for the wheels of the current state-of-the-art R718 chillers.

CHAPTER 11 : CONCLUSION

As described by this thesis, the advantages of the use of R718 are vast. These include environmental and economic benefits. Using traditional compression methods in conjunction with R718 and its unique characteristics, results in systems that are not economically feasible in the residential sector. To address this, an alternative compressor configuration is described along with its novel design for manufacture and integrated drive. The configuration is an axial, multi-stage, counter-rotating compressor with a woven composite impeller.

The woven impeller manufacturing method allows for several desirable characteristics. In addition to low-cost and rapid manufacturing, this design allows for a multitude of shapes, number of blades, curved blades, inner to outer diameter ratios, and outer shrouds. Perhaps the most novel characteristic of the design is its ability to include an integrated motor. This involves the inclusion of electrical components in the wheel to eliminate the need for a separate drive, essentially making the impeller the electric motor itself. The two electric motor configurations explored were the induction machine and the permanent magnet motor.

The design and manufacture of the woven composite impeller was realized on an inexpensive modified CNC mill using Kevlar® fiber with a polymer matrix. These impellers were inexpensive to prototype and testing of these composite wheels is currently being pursued. This testing includes structural spin tests as well as its performance in a compression cycle.

As mentioned in Chapter 1, the primary purpose for the development of a woven composite impeller is envisioned to be incorporated in an economically priced chiller using R718. However, this technology may be employed in other applications beyond the immediate motivation of this research. These applications may include chillers using traditional refrigerants, as well as applications in automotive, aerospace, train, propulsion, power generation, pumping, ventilation, and many others.

It was a goal of the presented research to show the enabling technology that will make R718 a viable alternative to traditional refrigerants. This has been accomplished by showing the thermodynamic advantages of water as a refrigerant, as well as addressing the challenges of R718 with alternative compressor technology, namely an axial, multi-stage, counter-rotating compressor configuration that uses a woven composite impeller. The concept of designing for manufacture, and producing this woven impeller has been proven to be feasible and economical, and it is evident that additional efforts may soon make this technology available to the mass U.S. market.

CHAPTER 12 : RECOMMENDATIONS FOR FURTHER STUDY

In continuing the research presented in this thesis, the author has several recommendations for further study provided additional funding. The first is to continue with the accurate control of winding parameters. The first of this is undoubtedly the accuracy of the fiber placement while winding the woven impellers. This can be accomplished by a custom-built winding machine using a more precise CNC stage. In addition to this, a feed-back control system is favorable to observe and control the accuracy of the winding process.

Alternate winding methods are also an intriguing option that should be explored. This may include the use of several fiber tows interwoven like used in a sewing machine instead of using a single tow as previously discussed. Another winding concept has been developed by using two leader tools to "lay" the fiber in a straight line across the mandrel and into two slots. Methods like these as well as alternate tooling methods should be realized given time and funding.

As can be referenced in [25] and [28], parameters such as controlled tension and resin application are very important to composite characteristics. Because of this, it is recommended that a tension and resin control system be utilized during the winding process. The tension control could be as simple as a friction device to create a resisting torque on the fiber spool, or it is also recommended that tension be controlled by electric motors installed on the spool dictating the fiber delivery rate as well as torque. A system like this would also benefit from a feed-back control loop. For the resin control, it is recommended that the research continue with an approach currently being explored using a syringe system with accurately controlled actuators.

For testing the woven impeller, efforts should be made to continue to establish a structural spin test. This includes the use of the RC engine and high-speed routers discussed previously. Although additional funding may tempt the use of expensive outsourced spin testing, in-house high-speed capability is favorable, and will inevitably become a necessity. Initial experiments indicate the usefulness of a dynamic balancer along with a vacuum chamber to conduct spin tests and these items are currently being constructed. As always, when working with structural integrity experiments, all safety precautions should be met. These include a vacuum chamber capable of withstanding bursting composite parts.

As mentioned in the preface, this work was a broad proof of concept and not a specific optimization of a particular component of the technology. Having established that these principles can, in general, be employed to enable the motivating concept of R718, the ever-important, specific exploration of individual aspects of this research can now be conducted. These include the optimization of blade angles, surface features, pattern selection, motor design, bearing configurations, and such.

In terms of motor design, the concept an induction machine was generally proven as conveyed earlier. However, additional exploration should be given to the concept of the permanent magnet motor design. This includes the research of various magnetic materials as well as their integration into the woven impeller. In addition, research should also be conducted on the methods of magnetizing iron elements once integrated in the impeller.

In terms of enhancing the refrigeration cycle thermodynamically, studies presented in [4] indicate the usefulness of introducing a condensing wave rotor to the cycle. The 3-port condensing wave rotor (CWR) pressurizes, de-superheats, and condenses the refrigerant vapor in one dynamic process. Therefore it substitutes for 3 subsystems: *intercooler*, *one compressor stage*, & *condenser*. This greatly reduces the size and cost of a chiller. In addition, it can enhance the energy efficiency of a R718 chiller by additional 10% [4].

APPENDIX A. EXAMPLE OF CYCLE CALCULATION

		R134a		
Point 1			Point 1-Superheat	0
Temp.[°C]	5		Super Heat=	5
Pressure[Pa]	349751.1	349.7511	Pressure[Pa]	349751.1
entropy[kJ/kg.K]	1724.701	1.724701	entropy[kJ/kg.K]	1724.701
h[J/kg]	401557.2	401.5572	h[J/kg]	401557.2
Point 2				
	26.04513			
Tempis.[°C]	21.66858		h2i[kJ/kg]	411696
Pressure[Pa]	571792	571.792	ηis=	0.7
entropy[J/kg.K]	1724.701	1.724701		
h2[kJ/kg]	416041.2	416.0412		
Point 3			Point 3-Subcooling	0
Temp.[°C]	20		Temp.[°C]	20
Pressure[Pa]	571792	571.792	Pressure[Pa]	571792
entropy[kJ/kg.K]	1097.614	1.097614	entropy[kJ/kg.K]	
h[kJ/kg]	227857.1	227.8571	h[kJ/kg]	227857.1
Point 4				
Temp.[°C]	5			
Pressure[Pa]	349751.1	349.7511		
entropy[kJ/kg.K]	1100.217	1.100217		
h[kJ/kg]	227857.1	227.8571		
	401557.2	0.107993	1724.700744	
	206827.7	1724.701	1024.612775	
COP				
qL[kJ/kg.K]	173700			
wnet[kJ/kg.K]	14483.98			
COP=	11.99256			
Polytropic Efficiency				
			K=γ=	1.035793
alfa	0.034556		Π	1.634854
			ηis=	0.697448
ηpol=	0.7			

R718

Point 1			Point 1-Superheat	0
Temp.[°C]	5		Super Heat=	5
Pressure[Pa]	871.8345517	0.871835	Pressure[Pa]	871.8345517
entropy[J/kg.K]	9026.899498	9.026899	entropy[kJ/kg.K]	9026.899498
h[J/kg]	2510734.169	2510.734	h[J/kg]	2510734.169

Point 2					
Tempis.[°C]	120.1702265		h2i[kJ/kg]	2726725.791	
Pressure[Pa]	2336.56155	2.336562	ηis=	0.662971597	
entropy[J/kg.K]	9221.405519	9.221406			
h2[kJ/kg]	2726725.791	2726.726	Δh=	215991.6224	[kJ/kg]

Point 3			Point 3-Subcooling	0
Temp.[°C]	20		Temp.[°C]	20
Pressure[Pa]	2336.56155	2.336562	Pressure[Pa]	2336.56155
entropy[kJ/kg.K]	296.2975647	0.296298	entropy[kJ/kg.K]	296.2975647
h[kJ/kg]	83861.7474	83.86175	h[kJ/kg]	83861.7474

Point 4		
Temp.[°C]	5.000000003	
Pressure[Pa]	871.8345517	0.871835
entropy[kJ/kg.K]	302.1724583	0.302172
h[kJ/kg]	83861.7474	83.86175
	21006.72659	0.025246
	2510734.169	76.20553
COP		9026.899
qL[J/kg.K]	2426872.421	
wnet[J/kg.K]	215991.6224	
COP=	**11.23595626**	

Polytropic Efficiency			
		K=γ=	1.325
alfa	0.245283019	Π	2.680051559
		ηis=	0.662971597
ηpol=	0.7		

Calculation of K=γ		
T=	63.02065221	62.58511
P1=	1604.198051	1604.198
Cp=	1877.695135	
R=	461.5	
Cv=	1416.195135	
K=γ=	1.325873172	

APPENDIX B: EXAMPLE OF VISUAL BASIC CODE USED IN CYCLE

```
Sub IsoCOPwater()

Col = 20

COP = Range("F7")

Var = 1

Do While COP <= (Range("F7") + 8 * Range("F8"))

Row = 3

Range("C3") = 0

Range("C4") = Range("C3") + 5

Cells(Row - 2, Col + 1) = "COP="

Cells(Row - 1, Col + 1) = COP

Do While Range("C3") < 360 And Abs(Range("C4")) < 360

Worksheets("All").Range("C13").Goalseek _

    Goal:=COP, _

ChangingCell:=Worksheets("All").Range("C4")

If Var = 1 Then Cells(Row, Col) = Range("C3") -
Range("F12")

Cells(Row, Col + 1) = Range("C4") - Range("C3") - 2 *
Range("F12")

Range("C3") = Range("C3") + 1

Row = Row + 1

Loop

Var = 0

COP = COP + Range("F8")

Col = Col + 1
```

```
Loop

End Sub

Sub IsoCOP()

Clean

IsoCOPwater

Col = 8

COP = Range("F7")


Do While COP <= (Range("F7") + 8 * Range("F8"))

Row = 3

Range("C3") = Range("F4")

Range("C4") = Range("C3") + 5

Cells(Row - 2, Col + 1) = "COP="

Cells(Row - 1, Col + 1) = COP

Do While Range("C3") < Range("F5") And Abs(Range("C4")) <
Range("F5")


Worksheets("All").Range("C12").Goalseek _

    Goal:=COP, _

ChangingCell:=Worksheets("All").Range("C4")

RowMax = Row

If Abs(Range("C4")) < Range("F5") Then Cells(RowMax, 8) =
Range("C3") - Range("F13")

If Abs(Range("C4")) < Range("F5") Then Cells(Row, Col + 1)
= Range("C4") - Range("C3") - 2 * Range("F13")

Range("C3") = Range("C3") + 1

Row = Row + 1

Loop

Cells(Row - 2, Col + 1) = Range("G1")
```

```
Cells(Row - 3, Col + 1) = Range("G1")
COP = COP + Range("F8")
Col = Col + 1
Loop
End Sub


Sub MaxCOPLineRefrigerant()
MaxCOPLineWater
Col = 9
Do While Col < 18
Row = 3
Maxlift = 0

Do While Row < 200
If Cells(Row, Col) > Maxlift Then
Maxlift = Cells(Row, Col)
MaxT1 = Cells(Row, 8)
End If
Row = Row + 1
Loop
Cells(Col + 15, 2) = MaxT1
Cells(Col + 15, 3) = Maxlift
Col = Col + 1
Loop
End Sub
```

```
Sub MaxCOPLineWater()
Col = 21
Do While Col < 30
Row = 3
Maxlift = 0

Do While Row < 350
If Cells(Row, Col) > Maxlift Then
Maxlift = Cells(Row, Col)
MaxT1 = Cells(Row, 20)
End If
Row = Row + 1
Loop
Cells(Col + 13, 2) = MaxT1
Cells(Col + 13, 3) = Maxlift
Col = Col + 1
Loop
End Sub

Sub Intersection()
IntersectionCells
Col = 32
Do While Col < 42
Var = 10000
Row = 3
```

```
Do While Row < 200

If Abs(Cells(Row, Col)) < Var And Abs(Cells(Row, Col)) <> 0
Then

Inter = Cells(Row, 20)

Inter2 = Cells(Row, Col - 11)

Var = Abs(Cells(Row, Col))

End If

Row = Row + 1

Loop

Cells(Col + 13, 2) = Inter

Cells(Col + 13, 3) = Inter2

Col = Col + 1

Loop

End Sub



Sub IntersectionCells()

RRow = 3

Coll = 32

Do While Cells(RRow, 8) <> Range("T3")

RRow = RRow + 1

Loop


Do While Coll < 41

RRRow = 3

hold = RRow

Roww = hold

Do While RRRow < 200
```

```
Cells(RRRow, Coll) = Cells(RRRow, 20 + Coll - 31) -
Cells(Roww, 8 + Coll - 31)

RRRow = RRRow + 1

Roww = Roww + 1

Loop

Coll = Coll + 1

Loop

End Sub
```

APPENDIX C. COMPLETE PATTERN DESIGN TABLE

Number of Points	Pattern	Not Possible	Shape	N	di/do	Notes
5	1, skip 1		5-A			
5	1, skip 2		5-A			Sharp turns
5	2, skip 1		5-A			
5	2, skip 2	x				
5	3, skip 1	x				
5	3, skip 2		5-A			Sharp turns
5	4, skip 1		5-A			
5	4, skip 2		5-A			Sharp turns
6	1, skip 1	x				
6	1, skip 2	x				
6	1, skip 3		6-A	1	0.5	Sharp turns
6	2, skip 1	x				
6	2, skip 2		6-B	0	0	Stack-up in the center
6	2, skip 3	x				
6	3, skip 1		6-A	1	0.5	
6	3, skip 2	x				
6	3, skip 3		6-A	1	0.5	Sharp turns
6	4, skip 1	x				
6	4, skip 2		6-B	0	0	Stack-up in the center
6	4, skip 3	x				
6	5, skip 1		6-A	1	0.5	
6	5, skip 2		6-B	0	0	Solid outside for 3 separate sixths of the circuit, normal inside, stack-up in the center
6	5, skip 3	x				
7	1, skip 1		7-A	1.5	0.62349	
7	1, skip 2		7-B	0.5	0.22252	
7	1, skip 3		7-B	0.5	0.22252	
7	1, skip 4		7-A	1.5	0.62349	Sharp turns
7	2, skip 1		7-A	1.5	0.62349	
7	2, skip 2		7-B	0.5	0.22252	
7	2, skip 3		7-B	0.5	0.22252	
7	2, skip 4	x			0	
7	3, skip 1		7-A	1.5	0.62349	
7	3, skip 2		7-B	0.5	0.22252	
7	3, skip 3	x			0	
7	3, skip 4		7-A	1.5	0.62349	Sharp turns
7	4, skip 1		7-A	1.5	0.62349	
7	4, skip 2	x			0	
7	4, skip 3		7-B	0.5	0.22252	
7	4, skip 4		7-A	1.5	0.62349	Sharp turns
7	5, skip 1	x			0	
7	5, skip 2		7-B	0.5	0.22252	
7	5, skip 3		7-B	0.5	0.22252	
7	5, skip 4		7-A	1.5	0.62349	Sharp turns
7	6, skip 1		7-A	1.5	0.62349	
7	6, skip 2		7-B	0.5	0.22252	
7	6, skip 3		7-B	0.5	0.22252	
7	6, skip 4		7-A	1.5	0.62349	Sharp turns

Shapes:

5-A

6-A

6-B

7-A

7-B

APPENDIX C. COMPLETE PATTERN DESIGN TABLE

Number of Points	Pattern	Not Possible	Shape	N	di/do	Notes
5	1, skip 1		5-A			
5	1, skip 2		5-A			Sharp turns
5	2, skip 1		5-A			
5	2, skip 2	x				
5	3, skip 1	x				
5	3, skip 2		5-A			Sharp turns
5	4, skip 1		5-A			
5	4, skip 2		5-A			Sharp turns
6	1, skip 1	x				
6	1, skip 2	x				
6	1, skip 3		6-A	1	0.5	Sharp turns
6	2, skip 1	x				
6	2, skip 2		6-B	0	0	Stack-up in the center
6	2, skip 3	x				
6	3, skip 1		6-A	1	0.5	
6	3, skip 2	x				
6	3, skip 3		6-A	1	0.5	Sharp turns
6	4, skip 1	x				
6	4, skip 2		6-B	0	0	Stack-up in the center
6	4, skip 3	x				
6	5, skip 1		6-A	1	0.5	
6	5, skip 2		6-B	0	0	Solid outside for 3 separate sixths of the circuit, normal inside, stack-up in the center
6	5, skip 3	x				
7	1, skip 1		7-A	1.5	0.62349	
7	1, skip 2		7-B	0.5	0.22252	
7	1, skip 3		7-B	0.5	0.22252	
7	1, skip 4		7-A	1.5	0.62349	Sharp turns
7	2, skip 1		7-A	1.5	0.62349	
7	2, skip 2		7-B	0.5	0.22252	
7	2, skip 3		7-B	0.5	0.22252	
7	2, skip 4	x			0	
7	3, skip 1		7-A	1.5	0.62349	
7	3, skip 2		7-B	0.5	0.22252	
7	3, skip 3	x			0	
7	3, skip 4		7-A	1.5	0.62349	Sharp turns
7	4, skip 1		7-A	1.5	0.62349	
7	4, skip 2	x			0	
7	4, skip 3		7-B	0.5	0.22252	
7	4, skip 4		7-A	1.5	0.62349	Sharp turns
7	5, skip 1	x			0	
7	5, skip 2		7-B	0.5	0.22252	
7	5, skip 3		7-B	0.5	0.22252	
7	5, skip 4		7-A	1.5	0.62349	Sharp turns
7	6, skip 1		7-A	1.5	0.62349	
7	6, skip 2		7-B	0.5	0.22252	
7	6, skip 3		7-B	0.5	0.22252	
7	6, skip 4		7-A	1.5	0.62349	Sharp turns

Shapes:

5-A

6-A

6-B

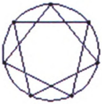

7-A

7-B

9 4, skip 2		9-B	1.5	0.5	
9 4, skip 3		9-C	0.5	0.17365	
9 4, skip 4	x			0	
9 4, skip 5		9-B	1.5	0.5	
9 4, skip 6		9-A	2.5	0.76604	Sharp turns
9 5, skip 1		9-A	2.5	0.76604	
9 5, skip 2		9-B	1.5	0.5	
9 5, skip 3	x			0	
9 5, skip 4		9-C	0.5	0.17365	
9 5, skip 5		9-B	1.5	0.5	
9 5, skip 6	x			0	
9 6, skip 1		9-A	2.5	0.76604	
9 6, skip 2	x			0	
9 6, skip 3		9-C	0.5	0.17365	
9 6, skip 4		9-C	0.5	0.17365	
9 6, skip 5	x			0	
9 6, skip 6		9-A	2.5	0.76604	Sharp turns
9 7, skip 1	x			0	
9 7, skip 2		9-B	1.5	0.5	
9 7, skip 3		9-C	0.5	0.17365	
9 7, skip 4	x			0	
9 7, skip 5		9-B	1.5	0.5	
9 7, skip 6		9-A	2.5	0.76604	Sharp turns
9 8, skip 1		9-A	2.5	0.76604	
9 8, skip 2		9-B	1.5	0.5	
9 8, skip 3	x			0	
9 8, skip 4		9-C	0.5	0.17365	
9 8, skip 5		9-B	1.5	0.5	
9 8, skip 6	x			0	
10 1, skip 1		10-A	3	0.80902	
10 1, skip 2	x			0	
10 1, skip 3	x			0	
10 1, skip 4	x			0	
10 1, skip 5		10-C	1	0.30902	
10 1, skip 6	x			0	
10 1, skip 7		10-A	3	0.80902	Sharp turns
10 2, skip 1	x			0	
10 2, skip 2	x			0	
10 2, skip 3	x			0	
10 2, skip 4		10-D	0	0	Stack-up in the center
10 2, skip 5	x			0	
10 2, skip 6		10-B	2	0.58779	
10 2, skip 7	x			0	
10 3, skip 1	x			0	
10 3, skip 2	x			0	
10 3, skip 3		10-C	1	0.30902	
10 3, skip 4		10-D	0	0	Solid outside for 5 separate tenths of the circuit, normal inside, stack-up in the center
10 3, skip 5		10-C	1	0.30902	

9-C

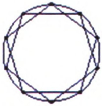

10-A

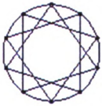

10-B

10 3, skip 6	x			0	
10 3, skip 7		10-A	3	0.80902	Sharp turns
10 4, skip 1	x			0	
10 4, skip 2		10-B	2	0.58779	
10 4, skip 3	x			0	
10 4, skip 4		10-D	0	0	Stack-up in the center
10 4, skip 5	x			0	
10 4, skip 6		10-B	2	0.58779	
10 4, skip 7	x			0	
10 5, skip 1		10-A	3	0.80902	
10 5, skip 2	x			0	
10 5, skip 3		10-C	1	0.30902	
10 5, skip 4	x			0	
10 5, skip 5		10-C	1	0.30902	
10 5, skip 6	x			0	
10 5, skip 7		10-A	3	0.80902	Sharp turns
10 6, skip 1	x			0	
10 6, skip 2		10-B	2	0.58779	
10 6, skip 3	x			0	
10 6, skip 4		10-D	0	0	Stack-up in the center
10 6, skip 5	x			0	
10 6, skip 6		10-B	2	0.58779	
10 6, skip 7	x			0	
10 7, skip 1		10-A	3	0.80902	
10 7, skip 2	x			0	
10 7, skip 3		10-C	1	0.30902	
10 7, skip 4		10-D	0	0	Solid outside for 5 separate tenths of the circuit, normal inside, stack-up in the center
10 7, skip 5		10-C	1	0.30902	
10 7, skip 6	x			0	
10 7, skip 7	x			0	
10 8, skip 1	x			0	
10 8, skip 2		10-B	2	0.58779	
10 8, skip 3	x			0	
10 8, skip 4		10-D	0	0	Stack-up in the center
10 8, skip 5	x			0	
10 8, skip 6	x			0	
10 8, skip 7	x			0	
10 9, skip 1		10-A	3	0.80902	
10 9, skip 2	x			0	
10 9, skip 3		10-C	1	0.30902	
10 9, skip 4		10-D	0	0	Solid outside for 5 separate tenths of the circuit, normal inside, stack-up in the center
10 9, skip 5	x			0	
10 9, skip 6	x			0	
10 9, skip 7		10-A	3	0.80902	Sharp turns

10-C

10-D

11 1, skip 1	11-A	3.5	0.84125	
11 1, skip 2	11-B	2.5	0.65486	
11 1, skip 3	11-C	1.5	0.41542	
11 1, skip 4	11-D	0.5	0.14231	
11 1, skip 5	11-D	0.5	0.14231	
11 1, skip 6	11-C	1.5	0.41542	
11 1, skip 7	11-B	2.5	0.65486	
11 1, skip 8	11-A	3.5	0.84125	Sharp turns
11 2, skip 1	11-A	3.5	0.84125	
11 2, skip 2	11-B	2.5	0.65486	
11 2, skip 3	11-C	1.5	0.41542	
11 2, skip 4	11-D	0.5	0.14231	
11 2, skip 5	11-D	0.5	0.14231	
11 2, skip 6	11-C	1.5	0.41542	
11 2, skip 7	11-B	2.5	0.65486	
11 2, skip 8	11-A	3.5	0.84125	Sharp turns
11 3, skip 1	11-A	3.5	0.84125	
11 3, skip 2	11-B	2.5	0.65486	
11 3, skip 3	11-C	1.5	0.41542	
11 3, skip 4	11-D	0.5	0.14231	
11 3, skip 5	11-D	0.5	0.14231	
11 3, skip 6	11-C	1.5	0.41542	
11 3, skip 7	11-B	2.5	0.65486	
11 3, skip 8	11-A	3.5	0.84125	Sharp turns
11 4, skip 1	11-A	3.5	0.84125	
11 4, skip 2	11-B	2.5	0.65486	
11 4, skip 3	11-C	1.5	0.41542	
11 4, skip 4	11-D	0.5	0.14231	
11 4, skip 5	11-D	0.5	0.14231	
11 4, skip 6	11-C	1.5	0.41542	
11 4, skip 7	11-B	2.5	0.65486	
11 4, skip 8	11-A	3.5	0.84125	Sharp turns
11 5, skip 1	11-A	3.5	0.84125	
11 5, skip 2	11-B	2.5	0.65486	
11 5, skip 3	11-C	1.5	0.41542	
11 5, skip 4	11-D	0.5	0.14231	
11 5, skip 5	11-D	0.5	0.14231	
11 5, skip 6	11-C	1.5	0.41542	
11 5, skip 7	11-B	2.5	0.65486	
11 5, skip 8	11-A	3.5	0.84125	Sharp turns
11 6, skip 1	11-A	3.5	0.84125	
11 6, skip 2	11-B	2.5	0.65486	
11 6, skip 3	11-C	1.5	0.41542	
11 6, skip 4	11-D	0.5	0.14231	
11 6, skip 5	11-D	0.5	0.14231	
11 6, skip 6	11-C	1.5	0.41542	
11 6, skip 7	11-B	2.5	0.65486	
11 6, skip 8	11-A	3.5	0.84125	Sharp turns

11-A

11-B

11-C

11-D

11 7, skip 1	11-A	3.5	0.84125	
11 7, skip 2	11-B	2.5	0.65486	
11 7, skip 3	11-C	1.5	0.41542	
11 7, skip 4	11-D	0.5	0.14231	
11 7, skip 5	11-D	0.5	0.14231	
11 7, skip 6	11-C	1.5	0.41542	
11 7, skip 7	11-B	2.5	0.65486	
11 7, skip 8	11-A	3.5	0.84125	Sharp turns
11 8, skip 1	11-A	3.5	0.84125	
11 8, skip 2	11-B	2.5	0.65486	
11 8, skip 3	11-C	1.5	0.41542	
11 8, skip 4	11-D	0.5	0.14231	
11 8, skip 5	11-D	0.5	0.14231	
11 8, skip 6	11-C	1.5	0.41542	
11 8, skip 7	11-B	2.5	0.65486	
11 8, skip 8	11-A	3.5	0.84125	Sharp turns
11 9, skip 1	11-A	3.5	0.84125	
11 9, skip 2	11-B	2.5	0.65486	
11 9, skip 3	11-C	1.5	0.41542	
11 9, skip 4	11-D	0.5	0.14231	
11 9, skip 5	11-D	0.5	0.14231	
11 9, skip 6	11-C	1.5	0.41542	
11 9, skip 7	11-B	2.5	0.65486	
11 9, skip 8	11-A	3.5	0.84125	Sharp turns
11 10, skip 1	11-A	3.5	0.84125	
11 10, skip 2	11-B	2.5	0.65486	
11 10, skip 3	11-C	1.5	0.41542	
11 10, skip 4	11-D	0.5	0.14231	
11 10, skip 5	11-D	0.5	0.14231	
11 10, skip 6	11-C	1.5	0.41542	
11 10, skip 7	11-B	2.5	0.65486	
11 10, skip 8	11-A	3.5	0.84125	Sharp turns

REFERENCES

1. **Dossat, Roy J. and Horan, Thomas J.** *Principles of Refrigeration- 5th ed.* Upper Saddle River, NJ : Pearson Education, Inc., 2002.

2. **Brown, D.** *Summer 2006 Electricity Supply and Demand Outlook.* s.l. : California Energy Commission, 2006.

3. **Cengel, Yunas A. and Boles, Michael A.** *Thermodynamics- An Engineering Approach- 3rd ed.* Boston, MA : McGraw-Hill, Inc., 1998.

4. *Preliminary Study of a Novel R718 Compression Refrigeration Cycle Using a 3- Port Condensing Wave Rotor.* **Amir A. Kharazi, P. Akbari, N. Mueller.** s.l. : ASME Journal of Engineering for Gas Turbines and Power, 2005, Vol. 127.

5. **S .E. Wright, T. Yoshinaka, B. A. Le Drew, N. C. D'Orsi.** *The Efficiency Limits of Water Vapor Compressors.* s.l. : ARTI-21CR/605-10010-01, 2000.

6. **Lachner, B., Nellis, G., and Reindl, D.** *The Use of Water Vapor as a Refrigerant Impact.* s.l. : ARTI-21CR/611-10080-01, 2004.

7. *Design of Compressors for Water as a Refrigerant.* **Mueller, N.** s.l. : ASHRAE Transactions, 2001, Vol. 107.

8. *Development of Large Capacity High Efficiency Mechanical Compression (MVC) Units.* **Zimmerman, Z.** s.l. : Desalination, 1994, Vol. 96.

9. *Turbo Water Chiller with Water as Refrigerant.* **Wobst, E., Kalitzin, N., Apley, R.** Purdue University : International Compressor Engineering Conference, 2005. C129.

10. **Burandt, B.** *Technische Information R718-Turbo-Kaltwassersatz.* Dresden, Germany : Institute fur Luft- und Kaltetechnik (ILK), 2004.

11. *Turbo chiller with water as a refrigerant.* **Albring, P., Heinrich, G.** Aarhus, Denmark : IIR, 1998. 4.

12. *The State of Art for Water Vapor Compressors and Cooling Plants Using Water as Refrigerant.* **Madsboll, M. S., Minds, G., Nyvad, J., and Elefsen, F.** Hanover : IIR, 1994.

13. *District Cooling with Water as Refrigerant Combined with Energy Storage Systems.* **Paul, J.** Oslso, Norway : IIF-IIR, 1998. B2, B1,E1,E2.

14. *Water Vapour Compression: Application and Outlook.* **Albring, P., Burandt B.,and Schenk, N.** 6, s.l. : KI Luft Kältetech DE, 2002, Vol. 38.

15. *New Age Water Chillers with Water as Refrigerant.* **Kühnl-Kinel, J.** Geneva, Switzerland : CERN, 1997.

16. **B., Burandt.** *Planungsdaten R718-Turbo-Kaltwassersatz (R718 chiller: data for planning).* Dresden, Germany : Institute fur Luft- und Kaltetechnik (ILK), 2004.

17. *Wasser als Kältemittel (water as a refrigerant).* Germany : BINE Informationsdienst, 2003. http://www.bine.info/pdf/publikation/bi0803internetx.pdf.

18. **Albring P., Müller N., et al.** *Turbo-compressor impeller for coolant. Patent No. 5,464,325* United States, 1994.

19. —. *Kältemittel-Turboverdichter (Refrigerant turbo-compressor). Reg.-No. 94108502.9* European Patent Registration, 1994.

20. —. *Radiallaufrad (Radial-flow impeller). DE 43 21 173 C2* Deutsche Patentschrift (German Patent), 1993.

21. *Water Chilling and Ice Making with Water as Refrigerant.* **Paul, J., Jahn E.** Washington, USA : International Conference on Ozon Protection Technologies, 1996.

22. **Aungier, R. H.** *Axial-Flow Compressors A Strategy for Aerodynamic Design and Analysis.* New York, NY : ASME Press, 2003.

23. **Dixon, S. L.** *Fluid Mechanics and Thermodynamics of Turbomachinery- 5th ed.* Burlington, MA : Elsevier Butterworth-Heinemann, 2005.

24. *A filament-wound structure technology Overview.* **Shen, Frank C.** s.l. : Materials Chemistry and Physics, 1995, Vol. 42.

25. **Chawla, Krishan K.** *Composite Materials- Science and Engineering- 2nd ed.* New York, NY : Springer Science and Business Media, Inc., 1998.

26. *Simulation and Production of Wound Impellers.* **Eyler, Allen and Mueller, Norbert.** Berlin, Germany : ASME Turbo Expo, 2008. GT 2008-51310.

27. *Preliminary Mechanical Analysis for Novel Woven/Wound Composite Axial-Compressor.* **Lahiri, A., Lindberg, B., Müller, N.** Seatle, Washington : ASME, 2007. IMECE 2007-42490.

28. *Influence of the filament winding tension on physical and mechanical properties of reinforced composites.* **P.Mertiny, F. Ellyin.** s.l. : Composites: Part A, 2002, Vol. 33.

29. *A comparative study of water as a refrigerant with some.* **Mueller, N., Kilicarslan, A.** s.l. : International Journal of Energy Research, 2005, Vol. 29.